

Simulating Fokker–Planck equations via mean field control of score-based normalizing flows

Mo Zhou^a, Stanley Osher^a, Wuchen Li^b

^a*Department of Mathematics, University of California, Los Angeles, 90095, CA, USA*

^b*Department of Mathematics, University of South Carolina, Columbia, 29208, SC, USA*

Abstract

The Fokker–Planck (FP) equation governs the evolution of densities for stochastic dynamics of physical systems, such as the Langevin dynamics and the Lorenz system. This work simulates FP equations through a mean field control (MFC) problem. We first formulate the FP equation as a continuity equation, where the velocity field consists of the drift function and the score function, i.e., the gradient of the logarithm of the density function. Next, we design a MFC problem that matches the velocity fields in a continuity equation with the ones in the FP equation. The score functions along deterministic trajectories are computed efficiently through the score-based normalizing flow, which only rely on the derivatives of the parameterized velocity fields. Numerical results, including Langevin dynamics, underdamped Langevin dynamics, and various chaotic systems, validate the effectiveness of our proposed algorithms. A convergence analysis is conducted for our algorithm on the FP equation of Ornstein–Uhlenbeck processes.

Keywords: Mean field control, Score-based normalizing flows, Flow matching, Lorenz systems, Underdamped Langevin dynamics.

2000 MSC: 34K35, 37N35, 58E25, 93C15, 93C20

1. Introduction

Simulating complex physical dynamics, especially chaotic systems, is a longstanding challenge [1]. Important examples include Langevin dynamics and the Lorenz system. These systems have attracted significant attention across statistical physics, stochastic control, and machine learning disciplines. The Fokker–Planck (FP) equation, which describes the evolution of probability densities, is studied to analyze these systems because it captures essential properties, such as the free energy dissipation [2, 3, 4, 5, 6]. In physics, the free energy is a physical quantity consisting of negative Boltzmann–Shannon entropy and linear potential energy of the negative logarithm of the invariant distribution. Mathematically, the free energy is a particular Lyapunov functional, which measures the closeness between the current density and invariant distributions. Designing fast, efficient, and accurate algorithms for FP equations that preserve the free energy dissipation is a central problem in the scientific computing and mathematical data science communities.

An algorithm for simulating the FP equation can be designed from a mean field control (MFC) problem. The MFC models the optimal control of interacting particles' trajectories by minimizing a cost functional, which has wide applications in finance [7], epidemic control

[6], and statistical physics [2]. In particular, the MFC for simulating the FP equation can be viewed as minimizing a discrepancy loss to learn the system’s dynamics, which is also known as the flow matching problem [8, 9, 10]. Here, the diffusion in the FP equation can be represented using the score function, which is the gradient of the logarithm of the probability density function. Using the score function, the FP equation can be reformulated as a continuity equation for a deterministic dynamic. As a result, one needs to solve an MFC problem involving the score function, which matches the velocity fields for the continuity equation. In practice, efficiently computing the score function along trajectories remains a computational challenge.

In recent years, the machine learning communities have introduced normalizing flows [11] and neural ordinary differential equations (ODEs) [12] for modeling and approximating deterministic dynamical systems. Normalizing flows construct a sequence of invertible push-forward maps that sequentially transfer one probability distribution into another, enabling flexible density estimation. Neural ODEs interpret the limit of residual neural networks as continuous-time dynamical systems. Despite their empirical success, these approaches’ scalability and convergence behaviors are still not fully understood, particularly in stochastic systems, such as complex physical and chaotic systems. Recently, new methods have been proposed to estimate score functions via deterministic ODEs governed by learned velocity fields [13, 14], which is known as the score-based normalizing flow. These models bridge stochastic dynamics with deterministic control through score-based transformations. *A natural question arises: Can we apply the score-based neural ODE to simulate the general FP equations of Langevin dynamics?*

This work proposes an MFC framework for simulating FP equations using score-based normalizing flows. We formulate flow matching for the FP equation as a MFC problem, where the stochastic dynamics are converted into deterministic ones using the score function. We introduce score-based neural ODEs and score-based normalizing flows as efficient tools for approximating score functions and modeling the evolution of probability densities. The deterministic velocity field is parameterized via neural networks and optimized by minimizing a variational discrepancy loss. Our framework enables accurate computation of key quantities such as the free energy and its dissipation. Numerical experiments on Langevin dynamics, underdamped Langevin dynamics (ULDs), and various chaotic systems validate the effectiveness of our proposed algorithms. These experiments confirm that our approach accurately captures the density evolution and reliably computes free energy and its dissipation over time. We provide a convergence analysis for the Ornstein—Uhlenbeck (OU) process.

Related works

The FP equation with gradient drift can be interpreted as a gradient flow of the relative entropy or free energy functional in the space of probability density with Wasserstein-2 metric [15, 16]. This gradient flow implies the dissipation property of free energy. For FP equations with non-gradient drifts, the free energies are still dissipative. In statistical physics, the MFC formulation is introduced to study the FP equation [2]. Mathematically, the theory of MFC and its counterpart, mean field games, has been developed extensively in [17, 18, 19, 20, 21]. It can be viewed as an optimal control problem [22] with dependence on distributions. These frameworks are particularly effective for modeling high-dimensional interacting systems. In

recent years, there has been growing interest in connecting MFC and optimal control with machine learning algorithms, including flow matching methods [23, 24, 25, 26, 27].

In approximating the FP equation for complex systems, the score function plays an important role. Various methods have been proposed to estimate the score function, including score matching [28, 29], kernel density estimations [30, 31], and denoising autoencoders [32, 33]. A score-based framework for generative modeling, namely time-reversible diffusion models, is introduced in [34]. This work is further extended to the Schrödinger bridges and stochastic control problems in [35]. Normalizing flows [11, 36] and neural ordinary differential equations (neural ODEs) [12] enable continuous-time density estimation by learning deterministic transport maps. Recent work on flow matching replaces exact log-likelihood objectives with trajectory-level matching losses between learned and target dynamics [37]. [38] introduced scalable generative models based on neural ODEs with exact change-of-variable computation. Different from existing literature, we designed an algorithm that uses score-based normalizing flow to simulate the FP equation.

The rest of this paper is organized as follows. In Section 2, we introduce the theoretical background, including the FP equation with entropy dissipation, formulation of flow matching for FP equations as an MFC problem, and the construction of score-based normalizing flow. In Section 3, we introduce the numerical algorithms for solving the flow matching problem. In Section 4, we present numerical results for examples, including the Langevin dynamics, underdamped Langevin dynamics (ULDs), and different chaotic systems to validate the effectiveness of our methods. In Section 5, we provide a convergence analysis for the Ornstein–Uhlenbeck (OU) process.

2. Theoretical background

In this section, we introduce the FP equation with its entropy dissipation property. Then we formulate flow matching for FP equations as MFC problems that involve the score functions. We introduce the score-based normalizing flow as an efficient way to compute the score function. We clarify some notations first. ∇_x denotes the gradient or Jacobian matrix of a function w.r.t. the variable $x \in \mathbb{R}^d$, where the gradient is always a column vector. $\nabla_x \cdot$, ∇_x^2 , and Δ_x are the divergence, the Hessian, and the Laplacian w.r.t. the variable x . $|\cdot|$ is the absolute value of a scalar, the l_2 norm of a vector, or the Frobenius norm of a matrix. $\text{Tr}(\cdot)$ denotes the trace of a square matrix. $\|\cdot\|_2$ denotes the l_2 operator norm of a matrix.

2.1. Fokker–Planck equation and entropy dissipation

Consider the FP equation

$$\partial_t \rho(t, x) + \nabla_x \cdot (\rho(t, x) b(x)) = \varepsilon \Delta_x \rho(t, x), \quad \rho(0, \cdot) = \rho_0, \quad (1)$$

where $b(x) : \mathbb{R}^d \rightarrow \mathbb{R}^d$ is the drift function and $\varepsilon > 0$ is the diffusion constant. $\rho(t, x)$ is the probability density function for the stochastic differential equation (SDE)

$$dx_t = b(x_t) dt + \sqrt{2\varepsilon} dW_t, \quad x_0 \sim \rho_0. \quad (2)$$

Since the FP equation (1) is time homogeneous, i.e. $b(x)$ does not depend on t , the FP equation admits a stationary distribution $\pi(x)$ under mild regularity condition such as the

Foster–Lyapunov criteria [39]. This $\pi(x)$ satisfies the stationary FP equation

$$\nabla_x \cdot (\pi(x)b(x)) = \varepsilon \Delta_x \pi(x).$$

We define the Kullback–Leibler (KL) divergence as

$$D_{\text{KL}}(\rho || \pi) := \int \rho(x) \log \frac{\rho(x)}{\pi(x)} dx.$$

Then, the FP equation satisfies the following entropy dissipation property.

Proposition 1 (Dissipation of relative entropy). *Let ρ be the solution to the FP equation (1), then*

$$\frac{d}{dt} D_{\text{KL}}(\rho(t, \cdot) || \pi) = -\varepsilon \int \left| \nabla_x \log \frac{\rho(t, x)}{\pi(x)} \right|^2 \rho(t, x) dx.$$

Here, $\nabla_x \log \frac{\rho(t, x)}{\pi(x)}$ is the relative score function.

2.2. Mean field control problem for Fokker–Planck equations

Flow matching for FP equation can be viewed as a MFC problem with a quadratic discrepancy cost

$$\inf_{v, \rho} \int_0^T \int_{\mathbb{R}^d} |v(t, x) - b(x)|^2 \rho(t, x) dx dt \quad (3)$$

subjected to the controlled FP equation

$$\partial_t \rho(t, x) + \nabla_x \cdot (\rho(t, x)v(t, x)) = \varepsilon \Delta_x \rho(t, x), \quad \rho(0, \cdot) = \rho_0, \quad (4)$$

where $T > 0$ is the terminal time. The controlled state dynamic is characterized by the FP equation (4), where one aims to match the target dynamic (1). The optimal control field to this MFC problem is $v^*(t, x) = b(x)$.

In this work, we reformulate the flow matching problem using the score function. By the identity $\nabla_x \rho / \rho = \nabla_x \log \rho$, we can rewrite the FP equation (1) as

$$\partial_t \rho(t, x) + \nabla_x \cdot [(b(x) - \varepsilon \nabla_x \log \rho(t, x)) \rho(t, x)] = 0. \quad (5)$$

Given the density function $\rho(t, x)$, we define the composed velocity field as $f(t, x) := b(x) - \varepsilon \nabla_x \log \rho(t, x)$, then the MFC problem for flow matching (3) can be rewritten as

$$\inf_{f, \rho} \int_0^T \int_{\mathbb{R}^d} |f(t, x) - b(x) + \varepsilon \nabla_x \log \rho(t, x)|^2 \rho(t, x) dx dt \quad (6)$$

subjected to the controlled continuity equation

$$\partial_t \rho(t, x) + \nabla_x \cdot (\rho(t, x)f(t, x)) = 0, \quad \rho(0, \cdot) = \rho_0. \quad (7)$$

The optimal velocity for this MFC is $f^*(t, x) = b(x) - \varepsilon \nabla_x \log \rho(t, x)$ where ρ is the solution to (1). The advantage of this formulation is that the dynamic is completely governed by a deterministic velocity field $f(t, x)$ without diffusion. Consequently, we are able to compute the reverse process, which has important applications in reversible diffusion [40] and generative models [34]. This formulation (6) also incurs a computational challenge—approximating the score function $\nabla_x \log \rho(t, x)$.

2.3. The score-based normalizing flow

We introduce the score-based normalizing flow in this section. Consider a probability flow, where the state process is governed by the ODE $\partial_t x_t = f(t, x_t)$ with random initialization $x_0 \sim \rho_0$. Let $\rho(t, \cdot)$ be the probability density function for x_t , then $\rho(t, x)$ satisfies the continuity equation (7). We denote $L_t = \rho(t, x_t)$, $l_t = \log \rho(t, x_t)$, $s_t = \nabla_x \log \rho(t, x_t)$, and $H_t = \nabla_x^2 \log \rho(t, x_t)$, then they satisfy the following ODE systems [13, 41, 14].

Proposition 2 (Score-based neural ODE systems). *Let x_t satisfy $\partial_t x_t = f(t, x_t)$. Then, $L_t = \rho(t, x_t)$, $l_t = \log \rho(t, x_t)$, $s_t = \nabla_x \log \rho(t, x_t)$, and $H_t = \nabla_x^2 \log \rho(t, x_t)$ satisfy*

$$\partial_t L_t = -\nabla_x \cdot f(t, x_t) L_t, \quad (8a)$$

$$\partial_t l_t = -\nabla_x \cdot f(t, x_t), \quad (8b)$$

$$\partial_t s_t = -\nabla_x f(t, x_t)^\top s_t - \nabla_x (\nabla_x \cdot f(t, x_t)), \quad (8c)$$

$$\partial_t H_t = -\sum_{i=1}^d s_{it} \nabla_x^2 f_i(t, x_t) - \nabla_x^2 (\nabla_x \cdot f(t, x_t)) - H_t \nabla_x f(t, x_t) - \nabla_x f(t, x_t)^\top H_t, \quad (8d)$$

where s_{it} and f_i are the i -th component of s_t and f respectively.

With f parametrized, we can compute the score function $s_t = \nabla_x \log \rho(t, x_t)$ along the trajectory efficiently [14].

3. Numerical algorithm

In this section, we present the numerical algorithm for solving the MFC problem (6). We parametrize the composed velocity field $f(t, x)$ as a multilayer perceptron (MLP) neural network $f_\theta(t, x)$, where θ denotes its parameters.

3.1. Numerical algorithm for flow matching

Let N_x and N_t denote the number of samples and the number of sub-intervals for time. We partition the time interval $[0, T]$ into N_t uniform subintervals with length $\Delta t = T/N_t$ and denote the discrete time points by $t_j = j\Delta t$ for $j = 0, \dots, N_t$. Given initial samples $\{x_0^{(n)}\}_{n=1}^{N_x}$ drawn i.i.d. from ρ_0 , we simulate the ODE dynamics (8) through

$$x_{t_{j+1}} = x_{t_j} + \Delta t f_\theta(t_j, x_{t_j}), \quad (9a)$$

$$L_{t_{j+1}} = L_{t_j} - \Delta t \nabla_x \cdot f_\theta(t_j, x_{t_j}) L_{t_j}, \quad (9b)$$

$$l_{t_{j+1}} = l_{t_j} - \Delta t \nabla_x \cdot f_\theta(t_j, x_{t_j}), \quad (9c)$$

$$s_{t_{j+1}} = s_{t_j} - \Delta t \left(\nabla_x f_\theta(t_j, x_{t_j})^\top s_{t_j} + \nabla_x (\nabla_x \cdot f_\theta(t_j, x_{t_j})) \right), \quad (9d)$$

$$H_{t_{j+1}} = H_{t_j} - \Delta t \left(\sum_{i=1}^d s_{it_j} \nabla_x^2 (f_\theta)_i(t_j, x_{t_j}) + \nabla_x^2 (\nabla_x \cdot f_\theta(t_j, x_{t_j})) \right. \\ \left. + H_{t_j} \nabla_x f_\theta(t_j, x_{t_j}) + \nabla_x f_\theta(t_j, x_{t_j})^\top H_{t_j} \right), \quad (9e)$$

where the derivatives of f is obtained through auto-differentiation. The variational objective (6) is then approximated using Monte Carlo sampling and discretization

$$L(\theta) = \frac{1}{N_x} \sum_{n=1}^{N_x} \sum_{j=0}^{N_t-1} \left| f_\theta(t_j, x_{t_j}^{(n)}) - b(x_{t_j}^{(n)}) + \varepsilon s_{t_j}^{(n)} \right|^2 \Delta t, \quad (10)$$

and minimized through gradient based optimization algorithms such as Adam method [42]. We conclude this method in Algorithm 1.

Algorithm 1 Flow matching solver through score-based normalizing flow

- 1: **Input:** Flow matching problem, neural network structure, number of steps N_{step} , learning rate, N_x, N_t
 - 2: **Output:** Approximated composed velocity field $f_\theta(\cdot, \cdot)$ for the MFC problem
 - 3: **Initialization:** Parameter θ for the composed neural network, $\Delta t = T/N_t$
 - 4: **for** step = 1, 2, \dots , N_{step} **do**
 - 5: Sample $\{x_0^{(n)}\}_{n=1}^{N_x}$ i.i.d. from ρ_0
 - 6: Compute $s_0^{(n)} = \nabla_x \log \rho_0(x_0^{(n)})$ for $n = 1, \dots, N_x$.
 - 7: Loss = 0
 - 8: **for** $j = 0, 1, \dots, N_t - 1$ **do**
 - 9: Loss = Loss + $\frac{1}{N_x} \sum_{n=1}^{N_x} \left| f_\theta(t_j, x_{t_j}^{(n)}) - b(x_{t_j}^{(n)}) + \varepsilon s_{t_j}^{(n)} \right|^2 \Delta t$ {update loss}
 - 10: $x_{t_{j+1}}^{(n)} = x_{t_j}^{(n)} + \Delta t f_\theta(t_j, x_{t_j}^{(n)})$ {update state}
 - 11: $s_{t_{j+1}}^{(n)} = s_{t_j}^{(n)} - \Delta t \left(\nabla_x f_\theta(t_j, x_{t_j}^{(n)})^\top s_{t_j}^{(n)} + \nabla_x (\nabla_x \cdot f_\theta(t_j, x_{t_j}^{(n)})) \right)$ {update score}
 - 12: **end for**
 - 13: Update θ through Adam method to minimize Loss
 - 14: **end for**
-

3.2. Numerical algorithms for flow matching over long horizons

For FP equations with long time horizons, it is challenging to characterize the entire dynamic using a single neural network. To address this, we adopt a multi-stage approach by decomposing the time interval $[0, T]$ into N_T stages (subintervals), each of length $T' := T/N_T$. We denote the stage endpoints by $T_m = mT'$ for $m = 1, \dots, N_T$, and define each stage interval as $I_m := [T_{m-1}, T_m]$.

For each stage I_m , we parameterize the velocity field by an independent neural network $f_m(t, x) := f_{\theta_m}(t, x)$. The flow matching model is trained sequentially for each stage. The initial states and score functions for stage I_m , are obtained by simulating the normalizing flow dynamics (9a) and (9d) using the previously trained network.

To improve efficiency, for stages $m = 2, \dots, N_T$, we initialize the parameter θ_m as θ_{m-1} , from the preceding stage, following a warm-start strategy [43]. This initialization provides a good starting point, often leading to faster convergence and reduced training iterations in subsequent stages. We summarize the algorithm for flow matching problems with long time horizons in Algorithm 2.

4. Numerical results

In this section, we present numerical results including Langevin dynamics, ULDs, and chaotic systems. All experiments were conducted on an NVIDIA TITAN V GPU using NVIDIA driver version 535.183.01 and CUDA 12.2. For all the problems, we apply a step size of $\Delta t = 0.01$.

4.1. Langevin dynamic

We consider the Langevin dynamic (2) with $d = 2n$ and $b(x) = -(I_d + cJ_d)\nabla_x V(x)$, where

$$J_d = \begin{bmatrix} 0 & I_n \\ -I_n & 0 \end{bmatrix}$$

is skew symmetric, $c = 0.5$, and $V(x)$ is the potential function such that $Z := \int_{\mathbb{R}^d} \exp(-V(x)/\varepsilon) dx$ is finite. The invariant distribution is $\pi(x) = \exp(-V(x)/\varepsilon)/Z$. We test Algorithm 1 with two potential functions: a quadratic function $V(x) = \frac{1}{2}|x|^2$ and a doublewell potential function $V(x) = \frac{1}{4}|x - c_1|^2|x - c_2|^2$, where c_1 and c_2 are vectors in \mathbb{R}^d with all entries being 1 and -1 respectively.

We define the Gibbs free energy functional as

$$D_V(\rho(t, \cdot)) = \int_{\mathbb{R}^d} \left(\log \rho(t, x) + \frac{1}{\varepsilon} V(x) \right) \rho(t, x) dx. \quad (11)$$

Then we can verify that

$$D_{\text{KL}}(\rho(t, \cdot) \parallel \pi) = D_V(\rho(t, \cdot)) + \log Z, \quad (12)$$

where Z is the partition function. By Proposition 1,

$$\frac{d}{dt} D_V(\rho(t, \cdot)) = -\varepsilon \int \left| \nabla_x \log \frac{\rho(t, x)}{\pi(x)} \right|^2 \rho(t, x) dx. \quad (13)$$

4.1.1. Langevin dynamic with quadratic potential

The numerical results for Langevin dynamic in 2 dimensions with a quadratic potential function $V(x) = \frac{1}{2}|x|^2$ and $\varepsilon = 0.5$ are presented in Figure 1. The first figure in the first row shows the training curve in log 10 scale. The discrepancy loss reaches an order of 10^{-4} . The shadow in the loss curve represents the standard deviation observed during 10 independent runs. The second and third figures on the first row show the free energy and its dissipation along time. The free energy (11) and its dissipation (13) are approximated numerically through

$$\widehat{D}_V(\rho(t_j, \cdot)) = \frac{1}{N_x} \sum_{n=1}^{N_x} \left(l_{t_j}^{(n)} + \frac{1}{\varepsilon} V(x_{t_j}^{(n)}) \right), \quad (14)$$

and

$$\widehat{\partial_t D}_V(\rho(t_j, \cdot)) = -\frac{\varepsilon}{N_x} \sum_{n=1}^{N_x} \left| s_{t_j}^{(n)} - \nabla_x \log \pi(x_{t_j}^{(n)}) \right|^2. \quad (15)$$

The approximation of the free energy over time, plotted in blue line in the second figure, is decaying and is align with the true energy in dashed orange line. The approximated

dissipation, plotted in blue in the third figure, is getting closer to 0, and is align with the true value. The visualization of f_θ at $t = 0$ is shown in the second row in Figure 1. The trained neural network accurately captures the true velocity field. We also report the errors for the neural network, the density and the score function:

$$\begin{aligned}\text{err}_f &= \frac{1}{N_x} \frac{1}{N_t + 1} \sum_{n=1}^{N_x} \sum_{j=0}^{N_t} \left| f(t_j, x_{t_j}^{(n)}; \theta) - f(t_j, x_{t_j}^{(n)}) \right|, \\ \text{err}_\rho &= \frac{1}{N_x} \frac{1}{N_t} \sum_{n=1}^{N_x} \sum_{j=1}^{N_t} \left| L_{t_j}^{(n)} - \rho(t_j, x_{t_j}^{(n)}) \right|, \\ \text{err}_s &= \frac{1}{N_x} \frac{1}{N_t} \sum_{n=1}^{N_x} \sum_{j=1}^{N_t} \left| s_{t_j}^{(n)} - \nabla_x \log \rho(t_j, x_{t_j}^{(n)}) \right|.\end{aligned}$$

Note that the errors for the density and score at $t = 0$ is 0, so we start at $j = 1$. After training, the errors achieve $\text{err}_f = 1.68 \times 10^{-2}$, $\text{err}_\rho = 6.93 \times 10^{-3}$, and $\text{err}_s = 1.06 \times 10^{-2}$. In addition, equation (12) provides a way to estimate the normalization constant Z . When T is sufficient large, $D_{\text{KL}}(\rho(T, \cdot) \parallel \pi) \approx 0$ and hence

$$Z \approx \exp(-D_V(\rho(T, \cdot))). \quad (16)$$

Using this formulation, we obtain an estimation $\exp(-\widehat{D}_V(\rho(T, \cdot))) = 3.1091$ (against the true value π), with a relative error of 1.03%.

4.1.2. Langevin dynamic with double-well potential

Next, we consider the Langevin dynamic with double-well potential function $V(x) = \frac{1}{4}|x - c_1|^2|x - c_2|^2$, where c_1 and c_2 are vectors in \mathbb{R}^d with all entries being 1 and -1 respectively.

The numerical results are shown in Figure 2. The first figure shows the scattered plot of the particles under the trained ODE dynamic (9a) at terminal time $T = 1$ and the level sets of the stationary density function $\pi(x)$. The second figure shows the 3D histogram plot for the particles at T and the surface plot for $\pi(x)$. We observe that x_t correctly demonstrates the bifurcation phenomenon and splits into two piles, which coincide with the invariant distribution. The third and fourth figures show the free energy and its dissipation, computed through (14) and (15). In addition, we also report that the estimated normalization constant through (16) is 1.81726, while a reference value obtained from Riemann sum is 1.83388. The relative error for this estimation is 0.906%.

4.2. Underdamped Langevin dynamic

The ULD is an SDE that models the motion of a particle subject to deterministic forces, random thermal fluctuations, and damping effects [44]. The dynamic is

$$\begin{cases} dx_t = v_t dt \\ dv_t = -(\gamma v_t + \nabla_x U(x_t)) dt + \sqrt{2\gamma\beta^{-1}} dW_t. \end{cases} \quad (17)$$

Here γ is the damping coefficient, β^{-1} is the temperature, and $U(x)$ is the potential function governing the deterministic forces. The FP equation for ULD with density function $\rho(t, x, v)$

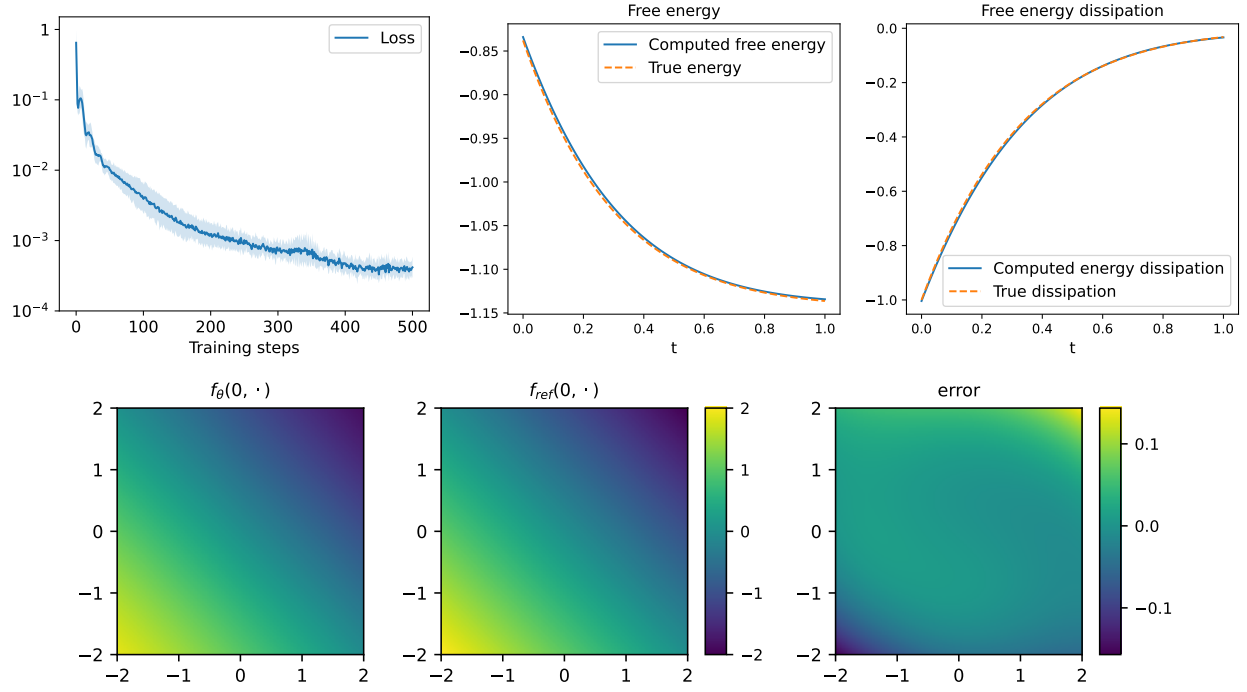


Figure 1: Numerical results for Langevin dynamic with quadratic potential. First row: the curve for loss function in log 10 scale, the curve for free energy and its dissipation along time. Second row: display the neural network, the reference solution, and the error at $t = 0$ as images.

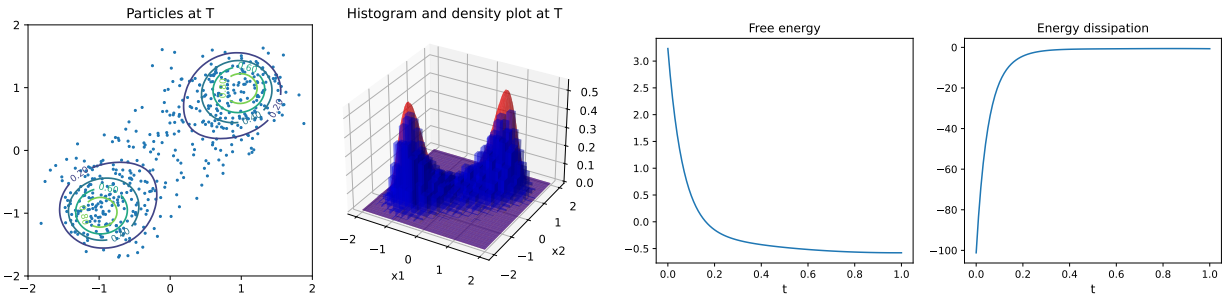


Figure 2: Numerical results for Langevin dynamic with double-well potential. The first two figures show the scattered plot and histogram of the particles at terminal time T . The third and fourth figures show the free energy and its dissipation.

is

$$\partial_t \rho + \nabla_x \cdot (v\rho) - \nabla_v \cdot ((\gamma v + \nabla_x U)\rho) = \frac{\gamma}{\beta} \Delta_v \rho. \quad (18)$$

Similar to (5), it can be rewritten as

$$\partial_t \rho + \nabla_x \cdot (v\rho) - \nabla_v \cdot \left((\gamma v + \nabla_x U + \frac{\gamma}{\beta} \nabla_v \log \rho) \rho \right) = 0.$$

We define the Hamiltonian as $H(x, v) = \frac{1}{2}|v|^2 + U(x)$. The stationary distribution for ULD is

$$\pi(x, v) = \frac{1}{Z} \exp \left[-\beta \left(\frac{1}{2}|v|^2 + U(x) \right) \right] = \frac{1}{Z} \exp(-\beta H(x, v)),$$

where $Z = \int_{\mathbb{R}^{2d}} \exp \left[-\beta \left(\frac{1}{2}|v|^2 + U(x) \right) \right] dx dv$ is the normalization constant. We define the free energy for a density function $\rho(x, v)$ as

$$D_H(\rho) = \int_{\mathbb{R}^{2d}} (\log \rho(x, v) + \beta H(x, v)) \rho(x, v) dx dv. \quad (19)$$

Then $D_{KL}(\rho(t, \cdot, \cdot) || \pi) = D_H(\rho(t, \cdot, \cdot)) + \log Z$. Similar to the previous subsection, this expression is used to approximate the normalization constant

$$Z \approx \exp(-D_H(\rho(T, \cdot, \cdot))), \quad (20)$$

where T is sufficiently large. We can also show the dissipation of energy along the dynamic.

Proposition 3 (Free energy dissipation of ULD). *The ULD satisfies the following energy dissipation formula*

$$\frac{d}{dt} D_H(\rho(t, \cdot, \cdot)) = -\frac{\gamma}{\beta} \int_{\mathbb{R}^{2d}} \rho(t, x, v) \left| \nabla_v \log \left(\frac{\rho(t, x, v)}{\pi(x, v)} \right) \right|^2 dx dv. \quad (21)$$

Since there is no noise for x_t , we only parametrize the composed velocity for v as $f_{v\theta}(t, x, v)$. We formulate the flow matching MFC problem for ULD as

$$\begin{aligned} & \inf_{f_v, \rho} \int_0^T \int_{\mathbb{R}^{2d}} |f_v(t, x, v) + (\gamma v + \nabla_x U(x)) + \gamma \beta^{-1} \nabla_v \log \rho(t, x, v)|^2 \rho(t, x, v) dx dv dt \\ & \text{s.t. } \partial_t \rho(t, x) + \nabla_x \cdot (\rho(t, x, v)v) + \nabla_v \cdot (\rho(t, x, v)f_v(t, x, v)) = 0, \quad \rho(0, \cdot, \cdot) = \rho_0. \end{aligned}$$

The stochastic van der Pol example in Section 4.3.3 is formulated in a similar manner.

We present the numerical results for a quadratic potential $U(x) = \frac{1}{2}|x|^2$ and double-well potential $U(x) = \frac{1}{4}|x - c_1|^2|x - c_2|^2$, which are the same as the potential functions in Section 4.1. The numerical implementation is in the same spirit as Algorithm 2 in Section 3, and the details are deferred to the Appendix.

4.2.1. Underdamped Langevin dynamic with quadratic potential

The numerical results for $U(x) = \frac{1}{2}|x|^2$ are presented in Figure 3. The first row shows the training curve, the free energy and its dissipation. The discrepancy loss is less than 1×10^{-3} . The approximation for the free energy and its dissipation accurately captures the reference value. The second and third rows in Figure 3 show the trained neural network at time 0 and $T = 5$, which accurately captures the true value. We also report that the errors for the neural network, density and score functions are $\text{err}_f = 1.58 \times 10^{-2}$, $\text{err}_\rho = 1.83 \times 10^{-3}$, $\text{err}_s = 3.73 \times 10^{-2}$. Additionally, the estimation for the normalization constant through (20) is 6.27844 against the true value 2π , with a relative error of 0.475%.

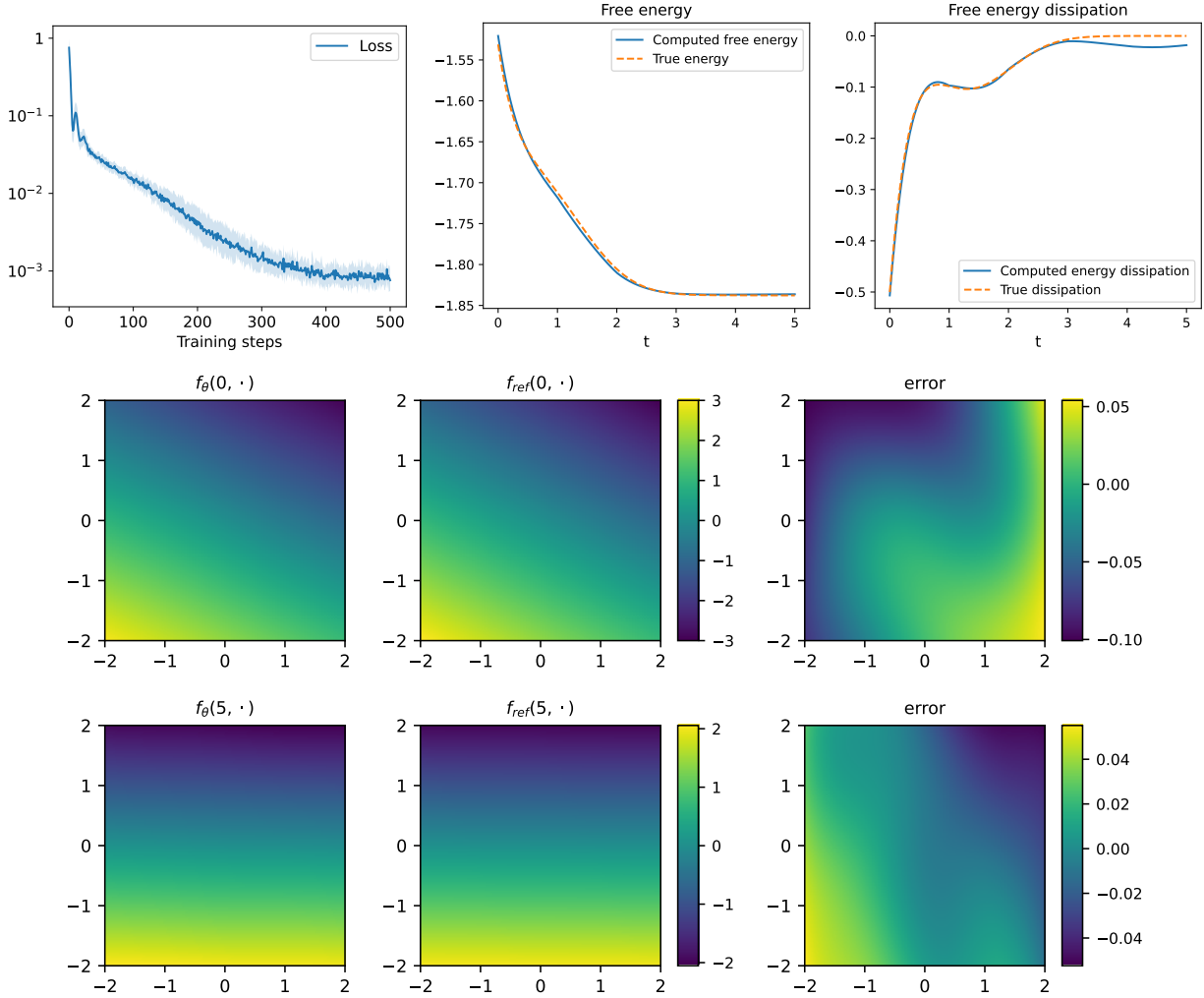


Figure 3: Underdamped Langevin dynamic with quadratic potential. First row: learning curve, computed evolution of the free energy, and its dissipation along time. Second and third rows: display the neural network, the reference solution, and the error as images at $t = 0$ and $t = 5$.

4.2.2. Underdamped Langevin dynamic with double-well potential

Next, we present the numerical result for underdamped Langevin dynamics with a double-well potential function. Since there is no reference solution, we compare the behavior of the

dynamic (9a) with the discretized Langevin dynamic. The numerical results is presented in Figure 4, where each figure shows the density and velocity field of the particles. The first row shows the deterministic probability flow dynamic under the trained velocity field. We observe that the deterministic dynamic correctly captures the density evolution of ULD dynamic. Additionally, the velocity field for the deterministic dynamic is more organized than the stochastic ULD due to the absence of Brownian motion.

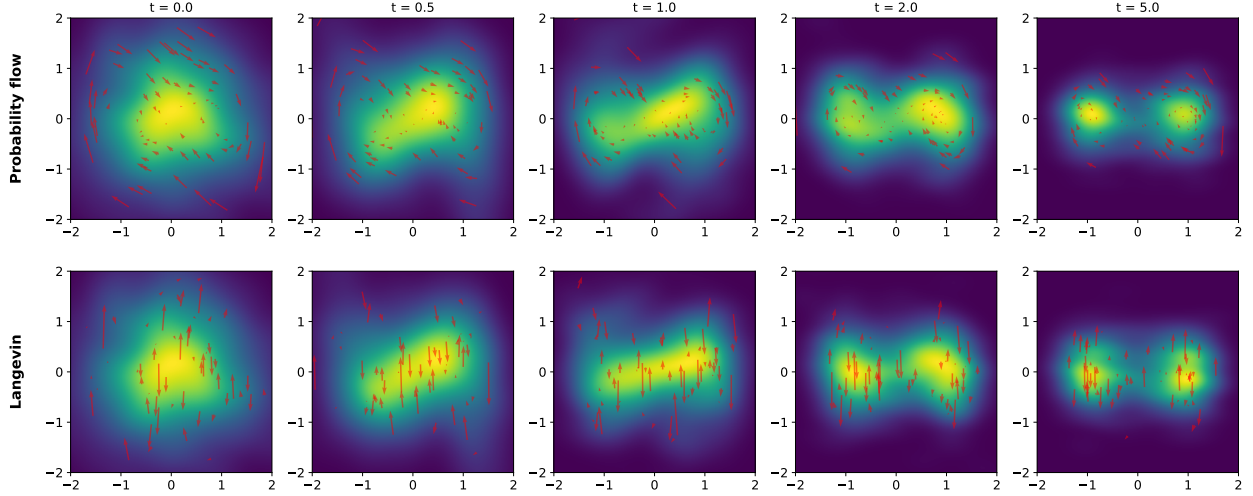


Figure 4: Density plot and velocity field for the Underdamped Langevin dynamic with double-well potential. First row: probability flow for deterministic dynamic with trained velocity field. Second row: stochastic dynamic (17).

4.3. Chaotic systems

We present numerical results for three chaotic systems in this section, including the Lorenz system, the Arctangent Lorenz system, and the stochastic van der Pol oscillator. These chaotic systems has been intensively studied [45]. In all three systems, we add a diffusion with $\varepsilon = 0.1$.

4.3.1. Lorenz system

The Lorenz 63 system

$$\begin{cases} \partial_t x_t = \sigma(y_t - x_t), \\ \partial_t y_t = x_t(\rho - z_t) - y_t, \\ \partial_t z_t = x_t y_t - \beta z_t, \end{cases} \quad (22)$$

was first introduced by Edward Lorenz for modeling atmospheric convection [46], with commonly used parameters $\sigma = 10$, $\rho = 28$, and $\beta = \frac{8}{3}$. We implement a scaling (with parameter $s = 0.2$) to the system (22) while preserving its chaotic behavior. In real world modeling, measurement noise or unpredictable external forcing is usually unavoidable. To reflect this, we add independent Brownian noise to each coordinate of the system with noise amplitude

$\varepsilon = 0.1$. The resulting scaled stochastic Lorenz system is

$$\begin{cases} dx_t = \sigma(y_t - x_t) dt + \sqrt{2\varepsilon} dW_t^x, \\ dy_t = (x_t(\rho - z_t/s) - y_t) dt + \sqrt{2\varepsilon} dW_t^y, \\ dz_t = (x_t y_t/s - \beta z_t) dt + \sqrt{2\varepsilon} dW_t^z. \end{cases} \quad (23)$$

Here, W_t^x , W_t^y , and W_t^z are independent standard Brownian for x , y , and z coordinates respectively. We remark that when $\varepsilon = 0$, i.e., in the absence of noise, the scaled Lorenz system behaves identically to the original unscaled dynamics (22). The scaling confines the trajectories within a more compact domain, which helps stabilize training by preventing divergence in the loss.

The numerical results are shown in Figure 5. Density plots and the corresponding velocity fields are shown at selected time points $t = 0, 0.3, 0.6, 1.0, 2.0, 5.0$, chosen to highlight key stages of the dynamical evolution. At the terminal time $T = 5$, the system appears to approach a stationary regime. The projections of the learned deterministic probability flow and the reference Langevin dynamics onto the x - y , x - z , and y - z planes are shown in rows 1-2, rows 3-4, and rows 5-6 of Figure 5, respectively. We observe that the deterministic probability flow correctly characterizes the density evolution of the stochastic Lorenz dynamic. Additionally, the velocity field for the deterministic dynamic is more organized compared with the stochastic dynamic, reflecting the absence of diffusion.

4.3.2. Arctangent Lorenz system

The Arctangent Lorenz system is studied in [1], where they have a scaling parameter 50. We scale their system by $s = 0.1$ and add a diffusion process as noise. Similar to the Lorenz example, we obtain the scaled stochastic Arctangent Lorenz system.

$$\begin{cases} dx_t = 50s \arctan(\sigma(y - x)/(50s)) dt + \sqrt{2\varepsilon} dW_t^x, \\ dy_t = 50s \arctan(x_t(\rho - 50sz_t) - 50sy_t) dt + \sqrt{2\varepsilon} dW_t^y, \\ dz_t = 50s \arctan((x_t y_t/s - \beta z_t)/(50s)) dt + \sqrt{2\varepsilon} dW_t^z. \end{cases} \quad (24)$$

The parameters are still $\sigma = 10$, $\rho = 28$, and $\beta = \frac{8}{3}$, and the noise level is $\varepsilon = 0.1$.

The numerical results at time stamps $t = 0, 0.5, 0.7, 1.0, 2.0, 5.0$ are presented in Figure 6, whose layout is the same as Figure 5. Similar to the Lorenz system, our trained velocity field f_θ is able to capture the stochastic process (24) using the deterministic dynamic, which is validated by the density plot. In addition, the deterministic dynamic demonstrates more structured velocity field, compared with the stochastic Langevin dynamic.

4.3.3. Stochastic van der Pol oscillator

The van der Pol oscillator was first invented in the 1920s to model electrical circuits containing vacuum tubes. Then it has become one of the most studied non-linear oscillator. A stochastic version of van der Pol oscillator is studied in [47, 48]. In this work, we consider the stochastic van der Pol oscillator

$$\begin{cases} dx_t = v_t dt \\ dv_t = \mu(1 - x_t^2)v_t dt + \sqrt{2\varepsilon} dW_t. \end{cases} \quad (25)$$

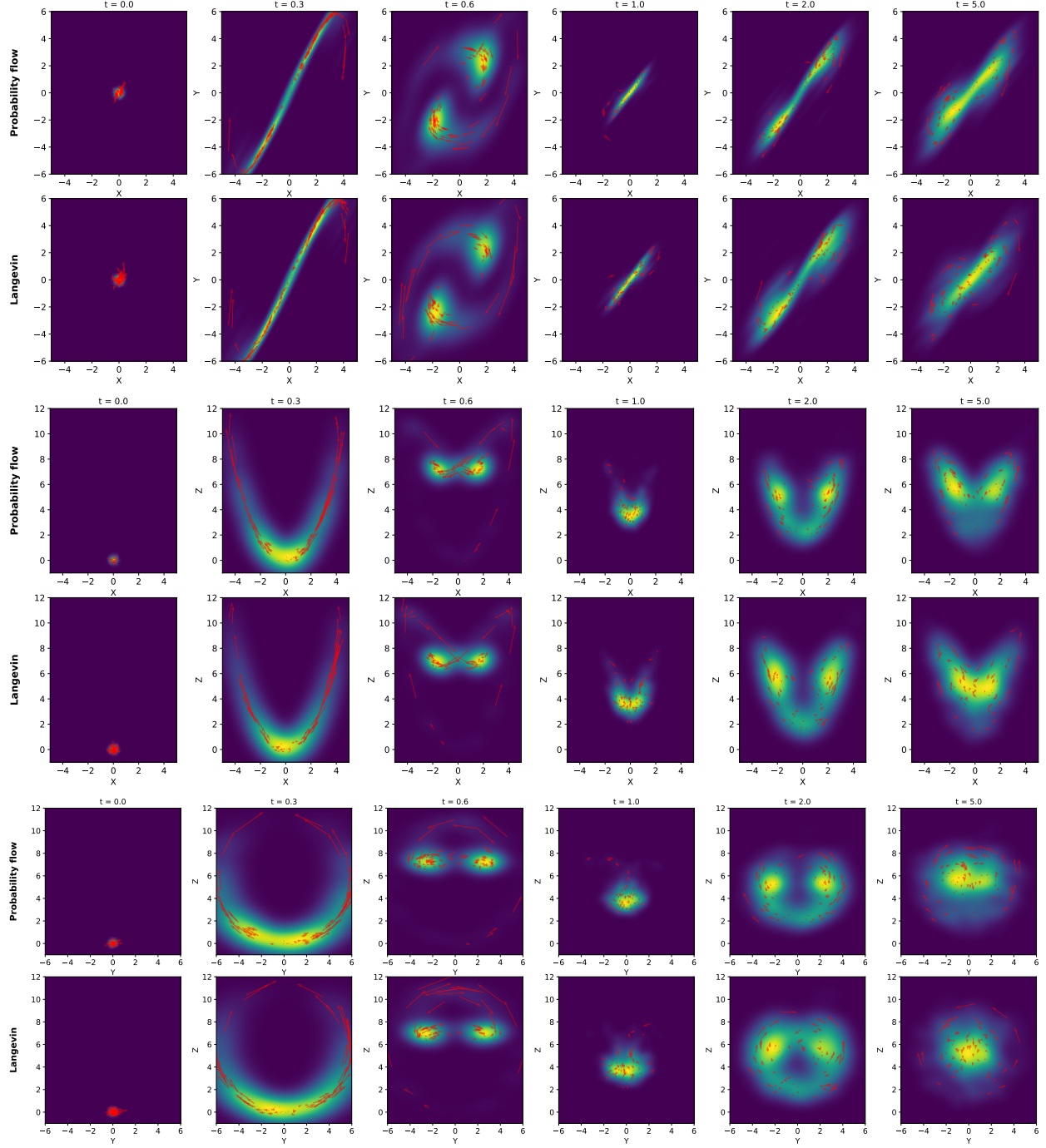


Figure 5: Density plot and velocity field for the stochastic Lorenz system. Rows 1, 3, 5: projection of the deterministic dynamic under trained velocity field into x - y , x - z , and y - z planes. Rows 2, 4, 6: projection of the stochastic dynamic (23) into x - y , x - z , and y - z planes.

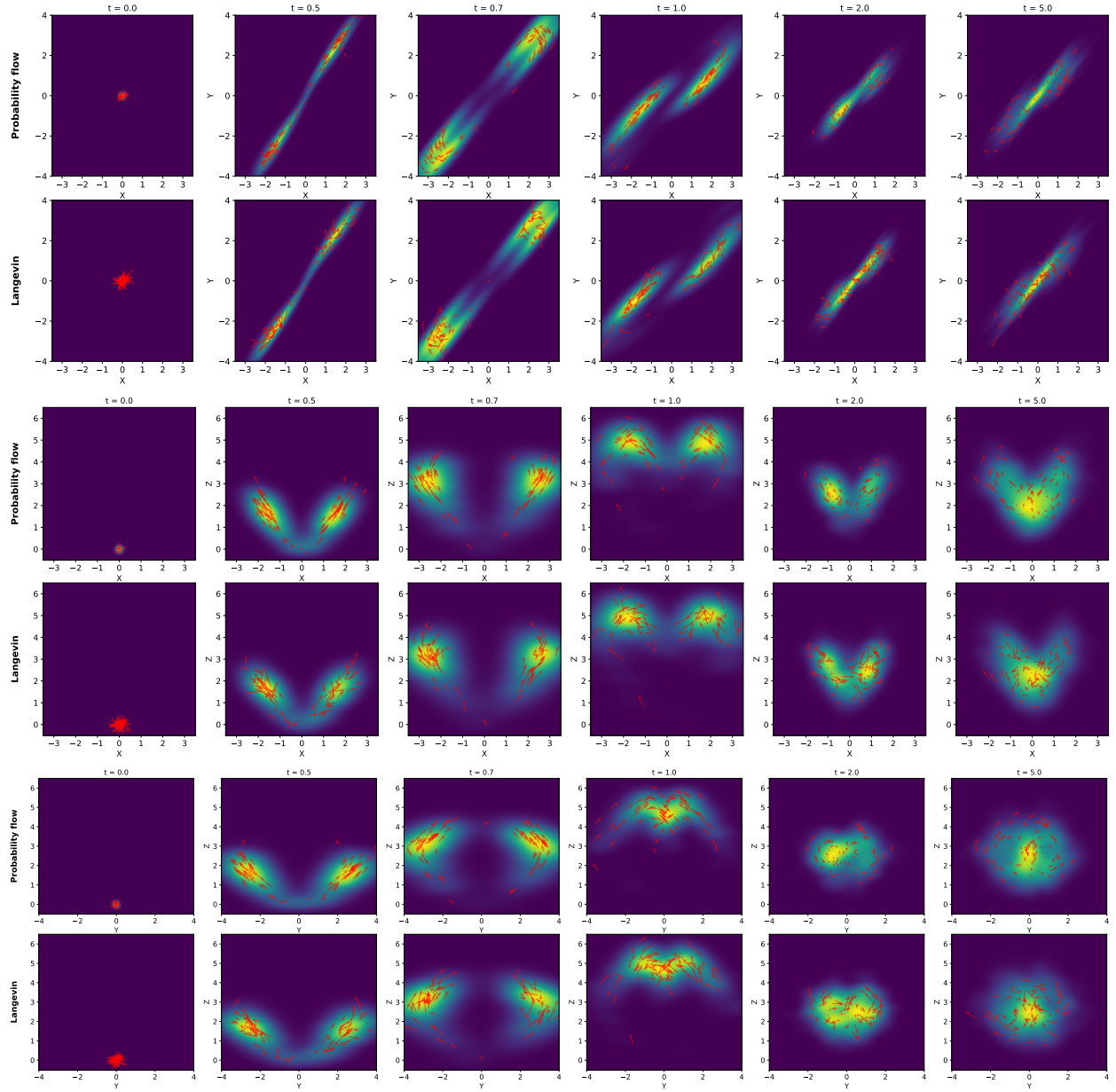


Figure 6: Density plot and velocity field for the stochastic Arctangent Lorenz system. Rows 1, 3, 5: projection of the deterministic dynamic under trained velocity field into x - y , x - z , and y - z planes. Rows 2, 4, 6: projection of the stochastic dynamic (24) into x - y , x - z , and y - z planes.

with a scalar parameter $\mu = 2.0$, and a diffusion parameter $\varepsilon = 0.1$. The numerical results are presented in Figure 7, where we pick the time stamps $t = 0.0, 0.2, 0.5, 1.0, 2.0$. The deterministic dynamic under the trained neural network correctly captures the density evolution while maintaining an organized velocity field.

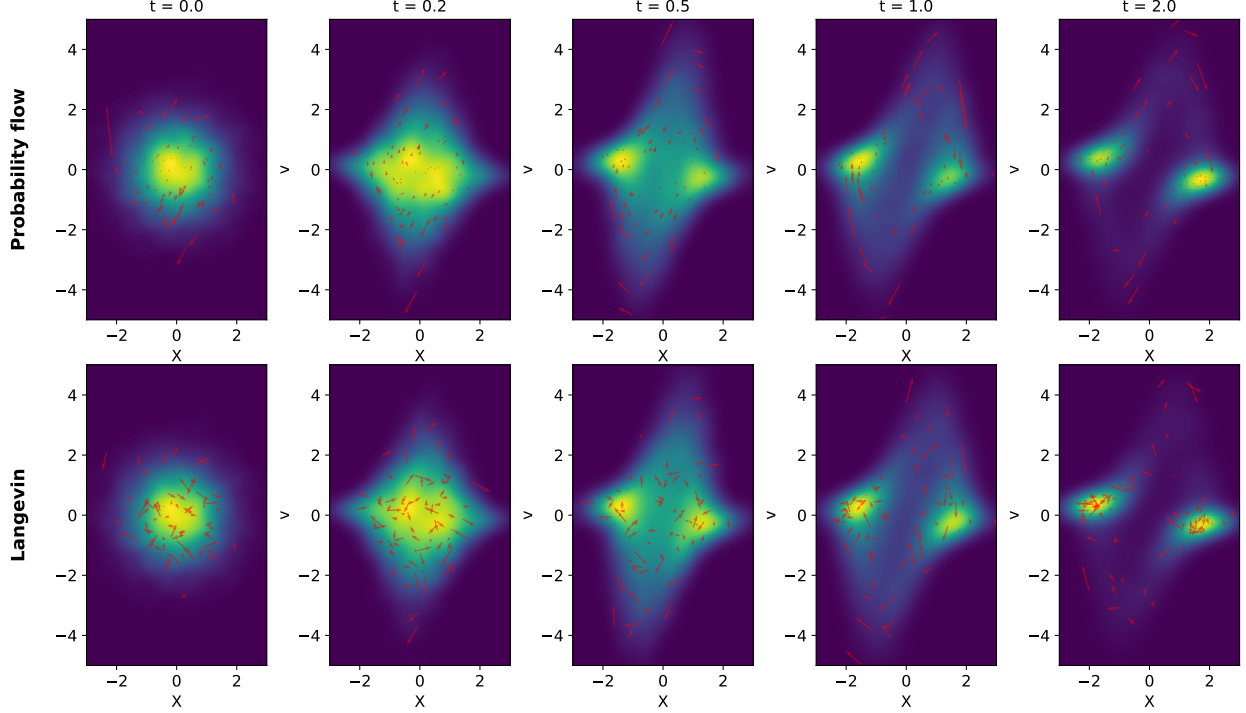


Figure 7: Numerical result for stochastic van der Pol dynamics. Row 1: deterministic dynamic under trained velocity field. Row 2: reference stochastic dynamic (25).

5. Convergence analysis

In this section, we present a convergence analysis for the flow matching problem of the OU process. For convergence analysis under general settings, we refer the readers to [49, 50, 51, 52, 53, 54, 55, 56]. Consider the OU process in \mathbb{R}^d

$$dx_t = b(x_t) dt + \sqrt{2\gamma} dW_t$$

with $x_0 \sim N(\mu_0, \Sigma_0)$. Here $b(x) = B_1x + b_0$, $B_1 \in \mathbb{R}^{d \times d}$, $b_0 \in \mathbb{R}^d$. The FP equation is

$$0 = \partial_t \rho + \nabla_x \cdot (\rho b(x)) - \gamma \Delta_x \rho = \partial_t \rho + \nabla_x \cdot (\rho(b(x) - \gamma \nabla_x \log \rho)).$$

We consider the linear parametrization $f(t, x; \theta) = \Theta_1(t)x + \theta_0(t)$, where $\Theta_1 : [0, T] \rightarrow \mathbb{R}^{d \times d}$, $\theta_0 : [0, T] \rightarrow \mathbb{R}^d$. We further discretize it into a one-step flow matching problem with forward Euler scheme. The parameter is $\theta = (\theta_0, \Theta_1) \in \mathbb{R}^d \times \mathbb{R}^{d \times d}$. The population loss (in expectation) is

$$\begin{aligned} L(\theta) &= \mathbb{E}_{x \sim N(\mu_0, \Sigma_0)} [|f(x; \theta) - b(x) + \gamma s(x)|^2] \\ &= \mathbb{E}_{x \sim N(\mu_0, \Sigma_0)} [|\Theta_1 x + \theta_0 - (B_1 x + b_0) - \gamma \Sigma_0^{-1}(x - \mu_0)|^2], \end{aligned} \quad (26)$$

where we omit $\Delta t = T$ in (10). Here, $s(x) = \nabla_x \log \rho(0, x) = -\Sigma_0^{-1}(x - \mu_0)$ is the score function at $t = 0$. With N_x samples $\{x^{(n)}\}_{n=1}^{N_x}$ drawn from ρ_0 , the empirical loss (with finite samples) is

$$\widehat{L}(\theta, \{x^{(n)}\}_{n=1}^{N_x}) = \frac{1}{N_x} \sum_{n=1}^{N_x} |\Theta_1 x^{(n)} + \theta_0 - (B_1 x^{(n)} + b_0) - \gamma \Sigma_0^{-1}(x^{(n)} - \mu_0)|^2.$$

We denote σ_0 is smallest eigenvalue of Σ_0 , and

$$\lambda_0 = \frac{1}{2} \left(1 + \sigma_0 + |\mu_0|^2 - \sqrt{(1 + \sigma_0 + |\mu_0|^2)^2 - 4\sigma_0} \right). \quad (27)$$

Then, the gradient descent algorithm

$$\theta^{(k+1)} = \theta^{(k)} - \eta \nabla_{\theta} \widehat{L}(\theta^{(k)}, \{x^{(n)}\}_{n=1}^{N_x})$$

has the following convergence property.

Theorem 1. *Let $\varepsilon > 0$ and $\delta \in (0, 1)$. Let the number of samples $N_x = \Omega(\lambda_0^{-2}(d - \log(\delta)))$. Assume the step size for gradient descent satisfies*

$$\eta \leq \frac{4}{3} / (8(1 + |\mu_0|^2) + 4 \|\Sigma_0\|_2 + \lambda_0).$$

Then, the gradient descent method on the empirical loss satisfies

$$\Pr \left(\widehat{L}(\theta^{(K)}, \{x^{(n)}\}_{n=1}^{N_x}) \leq \varepsilon \right) \geq 1 - \delta$$

after $K = \Omega(\log(\varepsilon^{-1})(\eta \lambda_0)^{-1})$ steps.

Proof. Step 1. We characterize the landscape of the population loss (26). We take derivative of the population loss and obtain the critical point equations

$$\begin{aligned} 0 &= \partial_{\theta_0} L(\theta) = 2\mathbb{E}_{x \sim N(\mu_0, \Sigma_0)} [\Theta_1 x + \theta_0 - (B_1 x + b_0) - \gamma \Sigma_0^{-1}(x - \mu_0)] \\ 0 &= \partial_{\Theta_1} L(\theta) = 2\mathbb{E}_{x \sim N(\mu_0, \Sigma_0)} [(\Theta_1 x + \theta_0 - (B_1 x + b_0) - \gamma \Sigma_0^{-1}(x - \mu_0)) x^\top]. \end{aligned}$$

The solution to this critical point system is the unique minimizer of $L(\theta)$, given by

$$\theta_0^* = b_0 - \gamma \Sigma_0^{-1} \mu_0 \quad \text{and} \quad \Theta_1^* = B_1 + \gamma \Sigma_0^{-1}.$$

Let $\theta_{0,j}$ be the j -th element of θ_0 and $\Theta_{1,j}$ be the j -th row of Θ_1 . Then the population loss can be written as $L(\theta) = \sum_{j=1}^d L_j(\theta)$, where

$$L_j(\theta) = \mathbb{E}_{x \sim N(\mu_0, \Sigma_0)} \left[(\Theta_{1,j} x + \theta_{0,j} - (B_{1,j} x + b_{0,j}) - \gamma (\Sigma_0^{-1})_{j,:} (x - \mu_0))^2 \right]$$

only depends on $\theta_{0,j}$ and $\Theta_{1,j}$. Therefore, in order to study the optimization landscape for $L(\theta)$, it is sufficient to study the optimization landscape for $L_j(\theta_{0,j}, \Theta_{1,j})$. Its critical point equations are

$$\begin{aligned} 0 &= \partial_{\theta_{0,j}} L_j = \mathbb{E}_{x \sim N(\mu_0, \Sigma_0)} [\Theta_{1,j} x + \theta_{0,j} - (B_{1,j} x + b_{0,j}) - \gamma (\Sigma_0^{-1})_{j,:} (x - \mu_0)] \\ &= \Theta_{1,j} \mu_0 + \theta_{0,j} - (B_{1,j} \mu_0 + b_{0,j}), \end{aligned}$$

and

$$\begin{aligned} 0 &= \partial_{\Theta_{1,j}} L_j = \mathbb{E}_{x \sim N(\mu_0, \Sigma_0)} \left[(\Theta_{1,j} x + \theta_{0,j} - (B_{1,j} x + b_{0,j}) - \gamma(\Sigma_0^{-1})_{j,:} (x - \mu_0)) x^\top \right] \\ &= \Theta_{1,j}(\Sigma_0 + \mu_0 \mu_0^\top) + \theta_{0,j} \mu_0^\top - (B_{1,j}(\Sigma_0 + \mu_0 \mu_0^\top) + b_{0,j} \mu_0^\top) - \gamma e_j^\top, \end{aligned}$$

where e_j is the j -th standard unit vector. The Hessian of L_j is

$$\nabla_{\theta_{0,j}, \Theta_{1,j}}^2 L_j(\theta_{0,j}, \Theta_{1,j}) = 2 \begin{bmatrix} 1 & \mu_0^\top \\ \mu_0 & \Sigma_0 + \mu_0 \mu_0^\top \end{bmatrix}. \quad (28)$$

Step 2. We estimate the Hessian for the population loss. First, we can verify through definition (27) that $\lambda_0 \in (0, 1]$. We claim that the smallest eigenvalue of the Hessian (28) is larger than or equal to λ_0 . If $\mu_0 = 0$, then $\lambda_0 = \min(1, \sigma_0)$, and claim is clear. If $\mu_0 \neq 0$, then $\lambda_0 \in (0, 1)$. For any $a \in \mathbb{R}$ and $b \in \mathbb{R}^d$, we have

$$\begin{aligned} &\frac{1}{2} [a, b^\top] \nabla_{\theta_{0,j}, \Theta_{1,j}}^2 L_j(\theta_{0,j}, \Theta_{1,j}) \begin{bmatrix} a \\ b \end{bmatrix} = [a, b^\top] \begin{bmatrix} 1 & \mu_0^\top \\ \mu_0 & \Sigma_0 + \mu_0 \mu_0^\top \end{bmatrix} \begin{bmatrix} a \\ b \end{bmatrix} \\ &= a^2 + 2ab^\top \mu_0 + b^\top (\Sigma_0 + \mu_0 \mu_0^\top) b \geq a^2 + 2ab^\top \mu_0 + b^\top (\sigma_0 I_d + \mu_0 \mu_0^\top) b \\ &= \left[(1 - \lambda_0) a^2 + 2ab^\top \mu_0 + \frac{1}{1 - \lambda_0} b^\top \mu_0 \mu_0^\top b \right] + \lambda_0 a^2 + b^\top \left(\sigma_0 I_d - \frac{\lambda_0}{1 - \lambda_0} \mu_0 \mu_0^\top \right) b \\ &\geq \frac{1}{1 - \lambda_0} ((1 - \lambda_0) a + \mu_0^\top b)^2 + \lambda_0 a^2 + \left(\sigma_0 - \frac{\lambda_0}{1 - \lambda_0} |\mu_0|^2 \right) |b|^2 \geq \lambda_0 (a^2 + |b|^2), \end{aligned}$$

where the last inequality is because $\lambda_0 = \sigma_0 - \frac{\lambda_0}{1 - \lambda_0} |\mu_0|^2$. Therefore, L_j is $2\lambda_0$ -strongly convex in $(\theta_{0,j}, \Theta_{1,j})$, which implies $L(\theta)$ is $2\lambda_0$ -strongly convex in (θ_0, Θ_1) . We also have the upper bound

$$\begin{aligned} &\frac{1}{2} [a, b^\top] \nabla_{\theta_{0,j}, \Theta_{1,j}}^2 L_j(\theta_{0,j}, \Theta_{1,j}) \begin{bmatrix} a \\ b \end{bmatrix} \\ &= a^2 + 2ab^\top \mu_0 + b^\top (\Sigma_0 + \mu_0 \mu_0^\top) b \\ &\leq 2a^2 + (\|\Sigma_0\|_2 + 2|\mu_0|^2) |b|^2, \end{aligned}$$

which implies $\left\| \nabla_{\theta_{0,j}, \Theta_{1,j}}^2 L_j \right\|_2 \leq 4(1 + |\mu_0|^2) + 2\|\Sigma_0\|_2$ and $\|\nabla_\theta^2 L(\theta)\|_2 \leq 4(1 + |\mu_0|^2) + 2\|\Sigma_0\|_2$.

Step 3. We study the optimization landscape for the empirical loss $\widehat{L}(\theta, \{x^{(n)}\}_{n=1}^{N_x})$. We denote $\widehat{\mu} := \frac{1}{N_x} \sum_{n=1}^{N_x} x^{(n)}$ and $\widehat{D} := \frac{1}{N_x} \sum_{n=1}^{N_x} x^{(n)} x^{(n)\top}$ the empirical mean and second order moments.

Similar to *step 2*, we can decompose the loss into $\widehat{L}(\theta, \{x^{(n)}\}_{n=1}^{N_x}) = \sum_{j=1}^d \widehat{L}_j(\theta, \{x^{(n)}\}_{n=1}^{N_x})$, where

$$\widehat{L}_j(\theta, \{x^{(n)}\}_{n=1}^{N_x}) = \frac{1}{N_x} \sum_{n=1}^{N_x} \left[(\Theta_{1,j} x^{(n)} + \theta_{0,j} - (B_{1,j} x^{(n)} + b_{0,j}) - \gamma(\Sigma_0^{-1})_{j,:} (x^{(n)} - \mu_0))^2 \right],$$

only depends on $\theta_{0,j}$ and $\Theta_{1,j}$. Taking derivatives, we obtain the critical point equations

$$\begin{aligned} 0 &= \partial_{\theta_{0,j}} \widehat{L}_j = \frac{2}{N_x} \sum_{n=1}^{N_x} [\Theta_{1,j} x^{(n)} + \theta_{0,j} - (B_{1,j} x^{(n)} + b_{0,j}) - \gamma(\Sigma_0^{-1})_{j,:} (x^{(n)} - \mu_0)] \\ &= \Theta_{1,j} \widehat{\mu} + \theta_{0,j} - (B_{1,j} \widehat{\mu} + b_{0,j}) - \gamma(\Sigma_0^{-1})_{j,:} (\widehat{\mu} - \mu_0), \end{aligned}$$

and

$$\begin{aligned} 0 &= \partial_{\Theta_{1,j}} \widehat{L}_j = \frac{2}{N_x} \sum_{n=1}^{N_x} [\Theta_{1,j} x^{(n)} + \theta_{0,j} - (B_{1,j} x^{(n)} + b_{0,j}) - \gamma(\Sigma_0^{-1})_{j,:}(x^{(n)} - \mu_0)] x_n^\top \\ &= \Theta_{1,j} \widehat{D} + \theta_{0,j} \widehat{\mu}^\top - (B_{1,j} \widehat{D} + b_{0,j} \widehat{\mu}^\top) - \gamma(\Sigma_0^{-1})_{j,:}(\widehat{D} - \mu_0 \widehat{\mu}^\top). \end{aligned}$$

The Hessian of L_j is

$$\nabla_{\theta_{0,j}, \Theta_{1,j}}^2 \widehat{L}_j(\theta_{0,j}, \Theta_{1,j}, \{x^{(n)}\}_{n=1}^{N_x}) = 2 \begin{bmatrix} 1 & \widehat{\mu}^\top \\ \widehat{\mu} & \widehat{D} \end{bmatrix}. \quad (29)$$

We observe that the critical point system has a unique solution $\theta_{0,j}^* = b_{0,j} - \gamma(\Sigma_0^{-1})_{j,:}\mu_0$, $\Theta_{1,j}^* = B_{1,j} + \gamma(\Sigma_0^{-1})_{j,:}$ if and only if the Hessian (29) is invertible. Let

$$\widehat{\Sigma} = \widehat{D} - \widehat{\mu} \widehat{\mu}^\top$$

be the empirical estimation for the covariance matrix. Then the invertibility of the Hessian (29) is equivalent to invertibility of $\widehat{\Sigma}$. When $N \geq d$, $\widehat{\Sigma}$ is invertible almost surely. In this case, we observe that the minimizer for the empirical loss is the same as the population loss.

Next, we apply the concentration theorem [57, Theorem 4.6.1]. Let $N_x = \Omega(\lambda_0^{-2}(d - \log(\delta)))$. Then, with probability $\geq 1 - \delta$, we have

$$\begin{aligned} \left\| \nabla_{\theta}^2 \widehat{L} - \nabla_{\theta}^2 L \right\|_2 &= \left\| 2 \begin{bmatrix} 1 & \widehat{\mu}^\top \\ \widehat{\mu} & \widehat{D} \end{bmatrix} - 2 \begin{bmatrix} 1 & \mu_0^\top \\ \mu_0 & \Sigma_0 + \mu_0 \mu_0^\top \end{bmatrix} \right\|_2 \\ &\leq C \frac{1}{\sqrt{N_x}} \left(\sqrt{d} + \sqrt{-\log \delta} \right) \leq \frac{1}{2} \lambda_0, \end{aligned}$$

where the last inequality is because $N_x = \Omega(\lambda_0^{-2}(d - \log(\delta)))$. Combining with the estimates in *step 2*, we obtain that

$$\nabla_{\theta}^2 \widehat{L} \geq \frac{3}{2} \lambda_0 I \quad \text{and} \quad \left\| \nabla_{\theta}^2 \widehat{L} \right\| \leq \frac{1}{2} \lambda_0 + 4(1 + |\mu_0|^2) + 2 \|\Sigma_0\|_2.$$

The first inequality implies that

$$\left| \nabla_{\theta} \widehat{L}(\theta) \right|^2 \geq 3\lambda_0 \left(\widehat{L}(\theta) - \widehat{L}(\theta^*) \right) = 3\lambda_0 \widehat{L}(\theta),$$

where we omit the input $\{x^{(n)}\}_{n=1}^{N_x}$ in \widehat{L} . Therefore, under the gradient descent algorithm

$$\theta^{(k+1)} = \theta^{(k)} - \eta \nabla_{\theta} \widehat{L}(\theta^{(k)}, \{x^{(n)}\}_{n=1}^{N_x}),$$

the loss function satisfies

$$\begin{aligned} \widehat{L}(\theta^{(k+1)}) &= \widehat{L}(\theta^{(k)} - \eta \nabla_{\theta} L(\theta^{(k)})) \\ &= \widehat{L}(\theta^{(k)}) - \eta \nabla_{\theta} L(\theta^{(k)})^\top \nabla_{\theta} L(\theta^{(k)}) + \frac{1}{2} \eta^2 \nabla_{\theta} L(\theta^{(k)})^\top \nabla_{\theta}^2 L(\xi^{(k)}) \nabla_{\theta} L(\theta^{(k)}) \\ &\leq \widehat{L}(\theta^{(k)}) - \eta |\nabla_{\theta} L(\theta^{(k)})|^2 + \frac{1}{2} \eta^2 \left(\frac{1}{2} \lambda_0 + 4(1 + |\mu_0|^2) + 2 \|\Sigma_0\|_2 \right) |\nabla_{\theta} L(\theta^{(k)})|^2 \\ &\leq \widehat{L}(\theta^{(k)}) - \frac{2}{3} \eta |\nabla_{\theta} L(\theta^{(k)})|^2 \leq (1 - 2\eta\lambda_0) \widehat{L}(\theta^{(k)}). \end{aligned}$$

Therefore,

$$\widehat{L}(\theta^{(K)}, \{x^{(n)}\}_{n=1}^{N_x}) \leq (1 - 2\eta\lambda_0)^K \widehat{L}(\theta^{(0)}, \{x^{(n)}\}_{n=1}^{N_x}) \leq \varepsilon.$$

□

We remark that the theorem does not include resampling in each step, because the optimal θ is the same for the empirical and population losses. We shall consider resampling for a general problem in the future work.

6. Conclusion and discussions

In this work, we formulate the flow matching for FP equations as an MFC problem and solve it through the score-based normalizing flow. We conduct a convergence analysis for the flow matching problem of the OU process and validate our algorithms on several examples, including Langevin dynamics, underdamped Langevin dynamics (ULDs), and several chaotic systems.

There are several interesting directions for future work. Firstly, it is worth investigating the impact of alternative time discretization schemes beyond the forward Euler method. We shall analyze how these schemes affect the accuracy and stability of flow-matching in scientific computing and machine learning problems, such as the score-based time-reversible diffusion models. Secondly, while our convergence analysis focuses on the OU process with a short time horizon, extending this analysis to broader classes of dynamics and longer horizons is a meaningful direction. Lastly, this work does not fully explore the dynamics of second-order score functions $H_t = \nabla_x^2 \log \rho(t, x_t)$. Understanding and designing fast algorithms for the second-order score function will be left for future study.

Appendix A. Derivation of formulas

Appendix A.1. Explicit formula for dissipation

In this subsection, we prove the dissipation properties for the free energy stated in the main text. First, we restate and prove Proposition 1.

Proposition 4 (Dissipation of relative entropy). *Let ρ be the solution to the FP equation (1), then*

$$\frac{d}{dt} D_{\text{KL}}(\rho(t, \cdot) \parallel \pi) = -\varepsilon \int \left| \nabla_x \log \frac{\rho(t, x)}{\pi(x)} \right|^2 \rho(t, x) dx.$$

Proof. We first make an orthogonal decomposition of the flow. We define the flux function as $\gamma(x) := \varepsilon \nabla_x \log \pi(x) - b(x)$, then $\nabla_x \cdot (\gamma(x) \pi(x)) = 0$. We can rewrite the FP equation (1) as

$$\partial_t \rho(t, x) = \varepsilon \nabla_x \cdot \left(\rho(t, x) \nabla_x \log \frac{\rho(t, x)}{\pi(x)} \right) + \nabla_x \cdot (\rho(t, x) \gamma(x)).$$

The reason we call it orthogonal decomposition is because

$$\begin{aligned}
& \int \gamma(x)^\top \nabla_x \log \left(\frac{\rho(t, x)}{\pi(x)} \right) \rho(t, x) dx = - \int \nabla_x \cdot (\gamma(x) \rho(t, x)) \log \left(\frac{\rho(t, x)}{\pi(x)} \right) dx \\
& = - \int \nabla_x \cdot \left(\gamma(x) \pi(x) \frac{\rho(t, x)}{\pi(x)} \right) \log \left(\frac{\rho(t, x)}{\pi(x)} \right) dx \\
& = - \int \gamma(x)^\top \pi(x) \nabla_x \left(\frac{\rho(t, x)}{\pi(x)} \right) \log \left(\frac{\rho(t, x)}{\pi(x)} \right) dx \\
& = \int \nabla_x \cdot \left(\gamma(x) \pi(x) \log \frac{\rho(t, x)}{\pi(x)} \right) \frac{\rho(t, x)}{\pi(x)} dx = \int \gamma(x)^\top \pi(x) \nabla_x \log \frac{\rho(t, x)}{\pi(x)} \frac{\rho(t, x)}{\pi(x)} dx \\
& = \int \gamma(x)^\top \pi(x) \nabla_x \left(\frac{\rho(t, x)}{\pi(x)} \right) dx = - \int \nabla_x \cdot (\gamma(x) \pi(x)) \frac{\rho(t, x)}{\pi(x)} = 0,
\end{aligned}$$

where we used the fact that $\nabla_x \cdot (\gamma(x) \pi(x)) = 0$. Therefore,

$$\begin{aligned}
& \frac{d}{dt} D_{\text{KL}}(\rho(t, \cdot) \parallel \pi) = \frac{d}{dt} \int \rho(t, x) \log \frac{\rho(t, x)}{\pi(x)} dx \\
& = \int \partial_t \rho(t, x) \left(\log \frac{\rho(t, x)}{\pi(x)} + 1 \right) dx = \int \partial_t \rho(t, x) \log \frac{\rho(t, x)}{\pi(x)} dx \\
& = \int \left[\varepsilon \nabla_x \cdot \left(\rho(t, x) \nabla_x \log \frac{\rho(t, x)}{\pi(x)} \right) + \nabla_x \cdot (\rho(t, x) \gamma(x)) \right] \log \frac{\rho(t, x)}{\pi(x)} dx \\
& = \int \varepsilon \nabla_x \cdot \left(\rho(t, x) \nabla_x \log \frac{\rho(t, x)}{\pi(x)} \right) \log \frac{\rho(t, x)}{\pi(x)} = -\varepsilon \int \left| \nabla_x \log \frac{\rho(t, x)}{\pi(x)} \right|^2 \rho(t, x) dx.
\end{aligned}$$

□

Next, we restate and prove Proposition 3.

Proposition 5 (Free energy dissipation of ULD). *The ULD satisfies the following energy dissipation formula*

$$\frac{d}{dt} D_H(\rho(t, \cdot, \cdot)) = -\frac{\gamma}{\beta} \int_{\mathbb{R}^{2d}} \rho(t, x, v) \left| \nabla_v \log \left(\frac{\rho(t, x, v)}{\pi(x, v)} \right) \right|^2 dx dv.$$

Proof. Let $\nabla = \nabla_{x,v}$ denote the full gradient. We denote

$$D = \frac{\gamma}{\beta} \begin{bmatrix} 0 & 0 \\ 0 & I_n \end{bmatrix} \text{ and recall that } J_d = \begin{bmatrix} 0 & I_n \\ -I_n & 0 \end{bmatrix}.$$

Then, the FP equation (18) can be rewritten as

$$\begin{aligned}
\partial_t \rho &= \nabla \cdot \left[\rho \left(\begin{bmatrix} 0 \\ \gamma \beta^{-1} (\nabla_v \log \rho + \beta v) \end{bmatrix} - \begin{bmatrix} v \\ -\nabla_x U(x) \end{bmatrix} \right) \right] \\
&= \nabla \cdot \left[\rho \left(D \nabla \log \frac{\rho}{\pi} - J_d \nabla \log \pi \right) \right] \\
&= \nabla \cdot \left[\rho (D + J_d) \nabla \log \frac{\rho}{\pi} \right],
\end{aligned}$$

where the last equality is because $\nabla \cdot (\rho J_d \nabla \log \rho) = \nabla \cdot (J_d \nabla \rho) = 0$. Therefore

$$\begin{aligned}
& \frac{d}{dt} D_H(\rho(t, \cdot, \cdot)) = \frac{d}{dt} D_{\text{KL}}(\rho(t, \cdot, \cdot) \parallel \pi) \\
&= \int_{\mathbb{R}^{2d}} \left(1 + \log \left(\frac{\rho(t, x, v)}{\pi(x, v)} \right) \right) \partial_t \rho(t, x, v) dx dv \\
&= \int_{\mathbb{R}^{2d}} \left(1 + \log \left(\frac{\rho(t, x, v)}{\pi(x, v)} \right) \right) \nabla \cdot \left[\rho(t, x, v) (D + J_d) \nabla \log \left(\frac{\rho(t, x, v)}{\pi(x, v)} \right) \right] dx dv \\
&= - \int_{\mathbb{R}^{2d}} \nabla \log \left(\frac{\rho(t, x, v)}{\pi(x, v)} \right)^\top \rho(t, x, v) (D + J_d) \nabla \log \left(\frac{\rho(t, x, v)}{\pi(x, v)} \right) dx dv \\
&= - \int_{\mathbb{R}^{2d}} \nabla \log \left(\frac{\rho(t, x, v)}{\pi(x, v)} \right)^\top \rho(t, x, v) D \nabla \log \left(\frac{\rho(t, x, v)}{\pi(x, v)} \right) dx dv \\
&= - \frac{\gamma}{\beta} \int_{\mathbb{R}^{2d}} \rho(t, x, v) \left| \nabla_v \log \left(\frac{\rho(t, x, v)}{\pi(x, v)} \right) \right|^2 dx dv.
\end{aligned}$$

□

Appendix A.2. Explicit solution for Gaussian case

For the Langevin dynamic

$$dx_t = -(I_d + cJ_d)x_t dt + \sqrt{2\varepsilon} dW_t$$

in Section 4.1.1 with Gaussian initialization $x_0 \sim N(0, \Sigma_0)$, the state remains Gaussian $x_t \sim N(0, \Sigma_t)$. The covariance matrix Σ_t satisfies

$$\partial_t \Sigma_t = A \Sigma_t + \Sigma_t A^\top + 2\varepsilon I_d,$$

where $A := -(I_d + cJ_d)$. If we further assume $\Sigma_0 = \delta I_{2n}$, then

$$\Sigma(t) = [e^{-2t}\delta + \varepsilon(1 - e^{-2t})] I_{2n}.$$

The corresponding score function is

$$\nabla_x \log \rho(t, x) = -\Sigma(t)^{-1}x = \frac{-x}{e^{-2t}\delta + \varepsilon(1 - e^{-2t})}.$$

The true composed velocity is

$$f(t, x) = b(x) - \varepsilon \nabla_x \log \rho(t, x) = Ax + \frac{\varepsilon x}{e^{-2t}\delta + \varepsilon(1 - e^{-2t})}.$$

We use these expressions to provide reference solutions. In the numerical experiments, we set $\delta = 1$. Note that $f(t, x)$ does not converge to 0 as $t \rightarrow \infty$ when $c \neq 0$. This makes the Langevin dynamic with non-gradient drift different from gradient drift.

For ULD with quadratic potential function $U(x) = \frac{1}{2}|x|^2$, we derive the this ODE for $d = 2$ with zero mean $(x_t, v_t) \sim N(0, \Sigma_t)$ for simplicity. A general Gaussian distribution with a non-zero mean can be derived in a similar way. We denote the entries of Σ_t by

$$\Sigma_t = \begin{bmatrix} \Sigma_t^{xx} & \Sigma_t^{xv} \\ \Sigma_t^{vx} & \Sigma_t^{vv} \end{bmatrix}$$

with $\Sigma_t^{xv} = \Sigma_t^{vx}$. Then we have

$$\partial_t \Sigma_t^{xx} = \partial_t \mathbb{E}[x_t^2] = 2\mathbb{E}[x_t v_t] = 2\Sigma_t^{xv}.$$

Since

$$d(x_t v_t) = [v_t^2 - (\gamma v_t + x_t)x_t] dt + \sqrt{2\gamma\beta^{-1}}x_t dW_t,$$

we have

$$\partial_t \Sigma_t^{xv} = \Sigma_t^{vv} - \gamma \Sigma_t^{xv} - \Sigma_t^{xx}.$$

Also, since

$$d(v_t^2) = [2\gamma\beta^{-1} - 2v_t(\gamma v_t + x_t)] dt + 2\sqrt{2\gamma\beta^{-1}}v_t dW_t,$$

we have

$$\partial_t \Sigma_t^{vv} = 2\gamma\beta^{-1} - 2\Sigma_t^{vv} - 2\Sigma_t^{xv}.$$

Combining the ODEs together, we get

$$\partial_t \begin{bmatrix} \Sigma_t^{xx} \\ \Sigma_t^{xv} \\ \Sigma_t^{vv} \end{bmatrix} = \begin{bmatrix} 0 & 2 & 0 \\ -1 & -\gamma & 1 \\ 0 & -2 & -2\gamma \end{bmatrix} \begin{bmatrix} \Sigma_t^{xx} \\ \Sigma_t^{xv} \\ \Sigma_t^{vv} \end{bmatrix} + \begin{bmatrix} 0 \\ 0 \\ 2\gamma\beta^{-1} \end{bmatrix}. \quad (\text{A.1})$$

In practice, we choose $\beta = \gamma = 1$ and approximate the solution to Σ_t using Runge—Kutta 4 (RK4) method. Figure A.8 shows the reference covariance evolution obtained from the RK4 scheme, together with the empirical estimation of the covariance with simulated 10^4 trajectories. We observe that the reference covariance coincides with its empirical estimation. Additionally, the empirical curve for Σ_t^{xx} is smoother because x_t does not have noise.

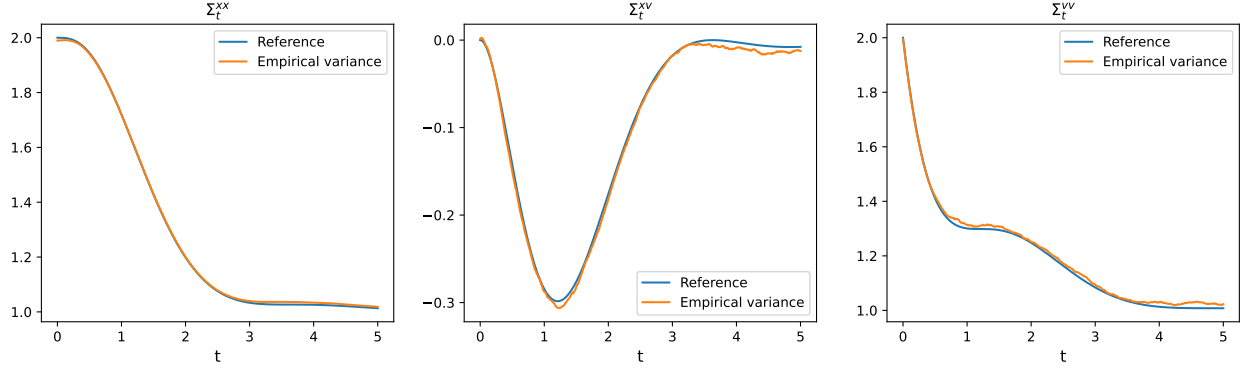


Figure A.8: Reference covariance evolution computed from RK4 scheme and empirical estimation.

Appendix A.3. Score-based normalizing flow for Underdamped Langevin dynamics

In this subsection, we derive the score-based normalizing flow for ULD. We denote the composed velocity for ULD as

$$f(t, x, v) = \begin{bmatrix} v \\ f_v(t, x, v) \end{bmatrix}.$$

Then, the probability flow dynamic for the state is

$$\partial_t \begin{bmatrix} x_t \\ v_t \end{bmatrix} = \begin{bmatrix} v_t \\ f_v(t, x_t, v_t) \end{bmatrix}.$$

By the ODE dynamics in Proposition 2, $L_t = \rho(t, x_t, v_t)$, $l_t = \log \rho(t, x_t, v_t)$, $s_t^x = \nabla_x \log \rho(t, x_t, v_t)$, and $s_t^v = \nabla_v \log \rho(t, x_t, v_t)$ satisfy

$$\begin{aligned} \partial_t L_t &= -\nabla_v \cdot f_v(t, x_t, v_t) L_t, \\ \partial_t l_t &= -\nabla_v \cdot f_v(t, x_t, v_t), \\ \partial_t \begin{bmatrix} s_t^x \\ s_t^v \end{bmatrix} &= - \begin{bmatrix} 0 & I_d \\ \nabla_x f_v & \nabla_v f_v \end{bmatrix}^\top \begin{bmatrix} s_t^x \\ s_t^v \end{bmatrix} - \begin{bmatrix} \nabla_x (\nabla_v \cdot f_v) \\ \nabla_v (\nabla_v \cdot f_v) \end{bmatrix}. \end{aligned} \tag{A.2}$$

In Gaussian case where $\begin{bmatrix} x_t \\ v_t \end{bmatrix} \sim N(0, \Sigma_t)$, the density function is

$$\rho(t, x, v) = (2\pi)^{-d} \det(\Sigma_t)^{-\frac{1}{2}} \exp \left(-\frac{1}{2} \begin{bmatrix} x \\ v \end{bmatrix}^\top \Sigma_t^{-1} \begin{bmatrix} x \\ v \end{bmatrix} \right),$$

where the covariance matrix Σ_t satisfies (A.1). Consequently, a reference solution to the composed velocity is

$$f(t, x, v) = \begin{bmatrix} v \\ -(x + \gamma v) \end{bmatrix} + \frac{\gamma}{\beta} \Sigma_t^{-1} \begin{bmatrix} x \\ v \end{bmatrix}.$$

We can also get the reference score function $s_t = -\Sigma_t^{-1} \begin{bmatrix} x_t \\ v_t \end{bmatrix}$. The reference free energy and its dissipation can be computed through (19) and (21).

Appendix B. Details for numerical implementations

We present the details for numerical implementation in this section.

Appendix B.1. Details for Underdamped Langevin dynamic

In the ULD example, the numerical discretization for the state and other dynamics in (A.2) are

$$\begin{aligned} x_{t_{j+1}} &= x_{t_j} + \Delta t v_{t_j}, \\ v_{t_{j+1}} &= v_{t_j} + \Delta t f_{v\theta}(t_j, x_{t_j}, v_{t_j}), \\ L_{t_{j+1}} &= L_{t_j} - \Delta t \nabla_x \cdot f_{v\theta}(t_j, x_{t_j}, v_{t_j}) L_{t_j}, \\ l_{t_{j+1}} &= l_{t_j} - \Delta t \nabla_x \cdot f_{v\theta}(t_j, x_{t_j}, v_{t_j}), \\ s_{t_{j+1}}^x &= s_{t_j}^x - \Delta t \left(\nabla_x f_{v\theta}(t_j, x_{t_j}, v_{t_j})^\top s_{t_j}^v + \nabla_x (\nabla_v \cdot f_{v\theta}(t_j, x_{t_j}, v_{t_j})) \right), \\ s_{t_{j+1}}^v &= s_{t_j}^v - \Delta t \left(s_{t_j}^x + \nabla_v f_{v\theta}(t_j, x_{t_j}, v_{t_j})^\top s_{t_j}^v + \nabla_v (\nabla_v \cdot f_{v\theta}(t_j, x_{t_j}, v_{t_j})) \right). \end{aligned}$$

As an analog to (14) and (15). An estimation of the free energy (19) and its dissipation (21) for ULD is obtained through

$$\widehat{D}_H(\rho(t_j, \cdot, \cdot)) = \frac{1}{N_x} \sum_{n=1}^{N_x} \left(l_{t_j}^{(n)} + \beta H(x_{t_j}^{(n)}, v_{t_j}^{(n)}) \right),$$

and

$$\widehat{\partial_t D}_H(\rho(t_j, \cdot, \cdot)) = -\frac{\gamma}{N_x \beta} \sum_{n=1}^{N_x} \left(s_{t_j}^{v(n)} - \nabla_v \log \pi(x_{t_j}^{(n)}, v_{t_j}^{(n)}) \right).$$

For ULD with a quadratic potential $U(x) = \frac{1}{2}|x|^2$, the state dynamic demonstrates a clear Hamiltonian structure. In this setting, we apply a symplectic scheme to enhance the stability, where we compute $x_{t_{j+1}} = x_{t_j} + \Delta t v_{t_{j+1}}$ after getting $v_{t_{j+1}}$. The update rules for other quantities remains unchanged. For general potential function, we keep using the forward Euler scheme. We conclude the numerical algorithm for ULD with quadratic and general potential in Algorithm 3 and 4. For both cases, we split intervals to overcome the issue of long time horizon. We train a neural network $f_m := f_{v\theta_m}$ within each stage as introduced in 3.2.

Appendix B.2. Hyperparameters and other details

In this subsection, we present the hyperparameters and other details for the numerical experiments.

Neural network

We parametrize the composed velocity field as the known drift field $b(x)$ added by a multilayer perceptron with tanh as the activation function. The drift field serve as a baseline that will benefit the training procedure. For all the experiments, we apply 2-layer networks with 100 neurons in the hidden layers.

Hyperparameters

For all the experiments, we apply a step size $\Delta t = 0.01$ and learning rate of 0.01. The other hyperparameters are presented in Table B.1.

Declaration of generative AI and AI-assisted technologies in the writing process

During the preparation of this work the authors used ChatGPT and Grammarly in order to polish the language of the article and correct grammatical mistakes. After using these tools, the authors reviewed and edited the content as needed and take full responsibility for the content of the published article.

Acknowledgements. M. Zhou’s work is partially supported by the AFOSR YIP award No. FA9550-23-1-0087. W. Li’s work is supported by the AFOSR YIP award No. FA9550-23-1-0087, NSF RTG: 2038080, and NSF DMS: 2245097.

Example	$(N_{\text{step0}}, N_{\text{step}})$	(T, N_T)	N_x	other parameters
Langevin OU	(, 500)	(1.0, 1)	500	$\varepsilon = 0.5, c = 0.5$
Langevin double-well	(, 500)	(1.0, 1)	500	$\varepsilon = 0.5, c = 0.5$
ULD Gaussian	(500, 200)	(5.0, 5)	1000	$\Sigma_0 = 2I_2, \beta = \gamma = 1$
ULD double-well	(500, 200)	(5.0, 25)	1000	$\Sigma_0 = I_2, \beta = \gamma = 1$
Lorenz	(500, 200)	(5.0, 25)	1000	$\varepsilon = 0.1, s = 0.2$
Arctangent Lorenz	(500, 200)	(5.0, 25)	1000	$\varepsilon = 0.1, s = 0.1$
Van der Pol	(500, 200)	(2.0, 10)	1000	$\varepsilon = 0.1, \mu = 2.0$

Table B.1: Hyperparameters for the numerical examples. c is the coefficient for anti-symmetry part of the drift function. N_T is the number of subintervals that we partition into. ε is the noise level. s is the scaling parameter introduced in Section 4.3.

References

- [1] Y. Yang, L. Nurbekyan, E. Negrini, R. Martin, M. Pasha, Optimal transport for parameter identification of chaotic dynamics via invariant measures, *SIAM Journal on Applied Dynamical Systems* 22 (1) (2023) 269–310.
- [2] L. Bertini, A. De Sole, D. Gabrielli, G. Jona-Lasinio, C. Landim, Macroscopic fluctuation theory, *Reviews of Modern Physics* 87 (2) (2015) 593–636.
- [3] S.-i. Amari, *Information geometry and its applications*, Vol. 194, Springer, 2016.
- [4] W. Li, J. Lu, L. Wang, Fisher information regularization schemes for wasserstein gradient flows, *Journal of Computational Physics* 416 (2020) 109449.
- [5] M. te Vrugt, H. Löwen, R. Wittkowski, Classical dynamical density functional theory: from fundamentals to applications, *Advances in Physics* 69 (2) (2020) 121–247.
- [6] W. Lee, S. Liu, H. Tembine, W. Li, S. Osher, Controlling propagation of epidemics via mean-field control, *SIAM Journal on Applied Mathematics* 81 (1) (2021) 190–207.
- [7] R. Carmona, M. Laurière, et al., Deep learning for mean field games and mean field control with applications to finance, *arXiv preprint arXiv:2107.04568* 7 (2021).
- [8] L. Li, S. Hurault, J. M. Solomon, Self-consistent velocity matching of probability flows, *Advances in Neural Information Processing Systems* 36 (2023) 57038–57057.
- [9] M. S. Albergo, N. M. Boffi, E. Vanden-Eijnden, Stochastic interpolants: A unifying framework for flows and diffusions, *arXiv preprint arXiv:2303.08797* (2023).
- [10] M. Lindsey, Mne: overparametrized neural evolution with applications to diffusion processes and sampling, *arXiv preprint arXiv:2502.03645* (2025).
- [11] D. Rezende, S. Mohamed, Variational inference with normalizing flows, in: *International conference on machine learning*, PMLR, 2015, pp. 1530–1538.

- [12] R. T. Chen, Y. Rubanova, J. Bettencourt, D. K. Duvenaud, Neural ordinary differential equations, *Advances in neural information processing systems* 31 (2018).
- [13] Z. Shen, Z. Wang, S. Kale, A. Ribeiro, A. Karbasi, H. Hassani, Self-consistency of the Fokker Planck equation, in: *Conference on Learning Theory*, PMLR, 2022, pp. 817–841.
- [14] M. Zhou, S. Osher, W. Li, Score-based neural ordinary differential equations for computing mean field control problems, *arXiv preprint arXiv:2409.16471* (2024).
- [15] L. Ambrosio, N. Gigli, G. Savaré, *Gradient flows: in metric spaces and in the space of probability measures*, Springer Science & Business Media, 2008.
- [16] R. Jordan, D. Kinderlehrer, F. Otto, The variational formulation of the Fokker–Planck equation, *SIAM journal on mathematical analysis* 29 (1) (1998) 1–17.
- [17] R. Carmona, F. Delarue, et al., *Probabilistic theory of mean field games with applications I-II*, Springer, 2018.
- [18] A. Bensoussan, J. Frehse, P. Yam, et al., *Mean field games and mean field type control theory*, Vol. 101, Springer, 2013.
- [19] G. Albi, Y.-P. Choi, M. Fornasier, D. Kalise, Mean field control hierarchy, *Applied Mathematics & Optimization* 76 (2017) 93–135.
- [20] M. Fornasier, F. Solombrino, Mean-field optimal control, *ESAIM: Control, Optimisation and Calculus of Variations* 20 (4) (2014) 1123–1152.
- [21] J. Li, Stochastic maximum principle in the mean-field controls, *Automatica* 48 (2) (2012) 366–373.
- [22] J. Yong, X. Y. Zhou, *Stochastic controls: Hamiltonian systems and HJB equations*, Vol. 43, Springer Science & Business Media, 1999.
- [23] L. Ruthotto, S. J. Osher, W. Li, L. Nurbekyan, S. W. Fung, A machine learning framework for solving high-dimensional mean field game and mean field control problems, *Proceedings of the National Academy of Sciences* 117 (17) (2020) 9183–9193.
- [24] X. Guo, A. Hu, R. Xu, J. Zhang, Learning mean-field games, *Advances in neural information processing systems* 32 (2019).
- [25] R. Hu, M. Lauriere, Recent developments in machine learning methods for stochastic control and games, *arXiv preprint arXiv:2303.10257* (2023).
- [26] C. Reisinger, Y. Zhang, Rectified deep neural networks overcome the curse of dimensionality for nonsmooth value functions in zero-sum games of nonlinear stiff systems, *Analysis and Applications* 18 (06) (2020) 951–999.
- [27] K. Hu, Z. Ren, D. Šiška, Ł. Szpruch, Mean-field Langevin dynamics and energy landscape of neural networks, in: *Annales de l’Institut Henri Poincaré (B) Probabilités et statistiques*, Vol. 57, Institut Henri Poincaré, 2021, pp. 2043–2065.

- [28] A. Hyvärinen, P. Dayan, Estimation of non-normalized statistical models by score matching., *Journal of Machine Learning Research* 6 (4) (2005).
- [29] S. Lyu, Interpretation and generalization of score matching, in: *Proceedings of the Twenty-Fifth Conference on Uncertainty in Artificial Intelligence*, UAI '09, AUAI Press, Arlington, Virginia, USA, 2009, p. 359–366.
- [30] E. L. Epstein, R. Dwaraknath, T. Sornwanee, J. Winnicki, J. W. Liu, Score-Debiased Kernel Density Estimation, *arXiv preprint arXiv:2504.19084* (2025).
URL <https://arxiv.org/abs/2504.19084>
- [31] M. Zhou, S. Osher, W. Li, A deep learning algorithm for computing mean field control problems via forward-backward score dynamics, *arXiv preprint arXiv:2401.09547* (2024).
- [32] P. Vincent, H. Larochelle, Y. Bengio, P.-A. Manzagol, Extracting and composing robust features with denoising autoencoders, in: *Proceedings of the 25th international conference on Machine learning*, 2008, pp. 1096–1103.
- [33] P. Vincent, A connection between score matching and denoising autoencoders, *Neural computation* 23 (7) (2011) 1661–1674.
- [34] Y. Song, J. Sohl-Dickstein, D. P. Kingma, A. Kumar, S. Ermon, B. Poole, Score-based generative modeling through stochastic differential equations, in: *International Conference on Learning Representations*, 2021.
URL <https://openreview.net/forum?id=PxtIG12RRHS>
- [35] V. De Bortoli, J. Thornton, J. Heng, A. Doucet, Diffusion schrödinger bridge with applications to score-based generative modeling, *Advances in Neural Information Processing Systems* 34 (2021) 17695–17709.
- [36] G. Papamakarios, E. Nalisnick, D. J. Rezende, S. Mohamed, B. Lakshminarayanan, Normalizing flows for probabilistic modeling and inference, *Journal of Machine Learning Research* 22 (57) (2021) 1–64.
- [37] Y. Lipman, R. T. Q. Chen, H. Ben-Hamu, M. Nickel, M. Le, Flow Matching for Generative Modeling, in: *International Conference on Learning Representations*, 2023.
URL <https://openreview.net/forum?id=PqvMRDCJT9t>
- [38] W. Grathwohl, R. T. Chen, J. Bettencourt, I. Sutskever, D. Duvenaud, FFJORD: Free-form Continuous Dynamics for Scalable Reversible Generative Models, in: *International Conference on Learning Representations*, 2019.
- [39] S. P. Meyn, R. L. Tweedie, Stability of Markovian processes III: Foster–Lyapunov criteria for continuous-time processes, *Advances in Applied Probability* 25 (3) (1993) 518–548.
- [40] N. Agmon, A. Szabo, Theory of reversible diffusion-influenced reactions, *The Journal of Chemical Physics* 92 (9) (1990) 5270–5284.

- [41] N. M. Boffi, E. Vanden-Eijnden, Probability flow solution of the Fokker–Planck equation, *Machine Learning: Science and Technology* 4 (3) (2023) 035012.
- [42] D. P. Kingma, J. Ba, Adam: A method for stochastic optimization, in: Y. Bengio, Y. LeCun (Eds.), 3rd International Conference on Learning Representations, ICLR 2015, San Diego, CA, USA, May 7-9, 2015, Conference Track Proceedings, 2015.
- [43] M. Zhou, J. Han, M. Rachh, C. Borges, A neural network warm-start approach for the inverse acoustic obstacle scattering problem, *Journal of Computational Physics* 490 (2023) 112341.
- [44] X. Cheng, N. S. Chatterji, P. L. Bartlett, M. I. Jordan, Underdamped Langevin MCMC: A non-asymptotic analysis, in: Conference on learning theory, PMLR, 2018, pp. 300–323.
- [45] S. L. Brunton, J. L. Proctor, J. N. Kutz, Discovering governing equations from data by sparse identification of nonlinear dynamical systems, *Proceedings of the national academy of sciences* 113 (15) (2016) 3932–3937.
- [46] E. N. Lorenz, Deterministic nonperiodic flow 1, in: *Universality in Chaos*, 2nd edition, Routledge, 2017, pp. 367–378.
- [47] Y. Xu, R. Gu, H. Zhang, W. Xu, J. Duan, Stochastic bifurcations in a bistable duffing–van der Pol oscillator with colored noise, *Physical Review E—Statistical, Nonlinear, and Soft Matter Physics* 83 (5) (2011) 056215.
- [48] M. Zhou, J. Han, J. Lu, Actor-critic method for high dimensional static Hamilton–Jacobi–Bellman partial differential equations based on neural networks, *SIAM Journal on Scientific Computing* 43 (6) (2021) A4043–A4066.
- [49] J. Han, R. Hu, J. Long, Convergence of deep fictitious play for stochastic differential games, *arXiv preprint arXiv:2008.05519* (2020).
- [50] H. Gu, X. Guo, X. Wei, R. Xu, Mean-field controls with Q-learning for cooperative MARL: convergence and complexity analysis, *SIAM Journal on Mathematics of Data Science* 3 (4) (2021) 1168–1196.
- [51] R. Carmona, M. Laurière, Convergence analysis of machine learning algorithms for the numerical solution of mean field control and games I: The ergodic case, *SIAM Journal on Numerical Analysis* 59 (3) (2021) 1455–1485.
- [52] R. Carmona, M. Laurière, Convergence analysis of machine learning algorithms for the numerical solution of mean field control and games: II—the finite horizon case, *The Annals of Applied Probability* 32 (6) (2022) 4065–4105.
- [53] M. Zhou, J. Lu, A policy gradient framework for stochastic optimal control problems with global convergence guarantee, *arXiv preprint arXiv:2302.05816* (2023).

- [54] D. Sethi, D. Šiška, Y. Zhang, Entropy annealing for policy mirror descent in continuous time and space, arXiv preprint arXiv:2405.20250 (2024).
- [55] M. Zhou, J. Lu, Solving time-continuous stochastic optimal control problems: Algorithm design and convergence analysis of actor-critic flow, arXiv preprint arXiv:2402.17208 (2024).
- [56] J. Ma, G. Wang, J. Zhang, Convergence analysis for entropy-regularized control problems: A probabilistic approach, arXiv preprint arXiv:2406.10959 (2024).
- [57] R. Vershynin, High-dimensional probability: An introduction with applications in data science, Vol. 47, Cambridge university press, 2018.

Algorithm 2 Flow matching solver for long time horizon

```

1: Input: Flow matching problem, neural network structure for each stage, number of
   steps for the first stage  $N_{\text{step0}}$  and the following stages  $N_{\text{step}}$ , learning rates,  $N_x, N_t, N_T$ 
2: Output: Approximated composed velocity fields  $\{f_m(\cdot, \cdot)\}_{m=1}^{N_T}$  for the MFC problem
3: Initialization: Parameter  $\theta_1$  for the first neural network  $f_1(\cdot, \cdot)$ 
4: Apply Algorithm 1 to train  $f_1(\cdot, \cdot)$  for  $N_{\text{step0}}$  steps with  $\Delta t = T/(N_T N_t)$ .
5: for  $m = 2, 3, \dots, N_T$  do
6:   Initialize  $\theta_m$  as  $\theta_{m-1}$  from previous stage {warm-start}
7:   for  $\text{step} = 1, 2, \dots, N_{\text{step}}$  do
8:     Sample  $\{x_0^{(n)}\}_{n=1}^{N_x}$  i.i.d. from  $\rho_0$ 
9:     Compute  $s_0^{(n)} = \nabla_x \log \rho_0(x_0^{(n)})$  for  $n = 1, \dots, N_x$ .
10:    for  $m' = 1, \dots, m - 1$  do
11:       $t_0 = (m' - 1)T'$  {initial time for the stage}
12:      for  $j = 0, \dots, N_t - 1$  do
13:         $t_{j+1} = ((m' - 1)N_t + j + 1)\Delta t$  {set time stamp}
14:         $x_{t_{j+1}}^{(n)} = x_{t_j}^{(n)} + \Delta t f_{m'}(t_j, x_{t_j}^{(n)})$  {update state}
15:         $s_{t_{j+1}}^{(n)} = s_{t_j}^{(n)} - \Delta t \left( \nabla_x f_{m'}(t_j, x_{t_j}^{(n)})^\top s_{t_j}^{(n)} + \nabla_x (\nabla_x \cdot f_{m'}(t_j, x_{t_j}^{(n)})) \right)$  {update score}
16:      end for
17:    end for
18:    Loss = 0 {compute loss for stage  $m$ }
19:     $t_0 = (m - 1)T'$ 
20:    for  $j = 0, 1, \dots, N_t - 1$  do
21:      Loss = Loss +  $\frac{1}{N_x} \sum_{n=1}^{N_x} \left| f_m(t_j, x_{t_j}^{(n)}) - b(x_{t_j}^{(n)}) + \varepsilon s_{t_j}^{(n)} \right|^2 \Delta t$  {update loss}
22:       $t_{j+1} = ((m - 1)N_t + j + 1)\Delta t$  {set time stamp}
23:       $x_{t_{j+1}}^{(n)} = x_{t_j}^{(n)} + \Delta t f_m(t_j, x_{t_j}^{(n)})$  {update state}
24:       $s_{t_{j+1}}^{(n)} = s_{t_j}^{(n)} - \Delta t \left( \nabla_x f_m(t_j, x_{t_j}^{(n)})^\top s_{t_j}^{(n)} + \nabla_x (\nabla_x \cdot f_m(t_j, x_{t_j}^{(n)})) \right)$  {update score}
25:    end for
26:    Update  $\theta_m$  through Adam method to minimize Loss
27:  end for
28: end for

```

Algorithm 3 Flow matching solver for ULD with quadratic potential

```

1: Input: Parameter  $\beta, \gamma$ , neural network structure for each stage, number of steps for
   the first stage  $N_{\text{step0}}$  and the following stages  $N_{\text{step}}$ , learning rates,  $N_x, N_t, N_T$ 
2: Output: Approximated composed velocity fields  $\{f_m(\cdot, \cdot)\}_{m=1}^{N_T}$  for the MFC problem
3: Initialization: Parameter  $\theta_1$  for the first neural network  $f_1(\cdot, \cdot)$ ,  $\Delta t = T/(N_T N_t)$ 
4: for step = 1, 2, ...,  $N_{\text{step0}}$  do
5:   Loss = 0,  $t_0 = 0$ , Sample  $\{(x_0^{(n)}, v_0^{(n)})\}_{n=0}^{N_x}$  i.i.d. from  $\rho_0$ 
6:   Compute  $s_0^{x(n)} = \nabla_x \log \rho_0(x_0^{(n)}, v_0^{(n)})$  and  $s_0^{v(n)} = \nabla_v \log \rho_0(x_0^{(n)}, v_0^{(n)})$ 
7:   for  $j = 0, 1, \dots, N_t - 1$  do
8:     Loss = Loss +  $\frac{1}{N_x} \sum_{n=1}^{N_x} |f_1(t_j, x_{t_j}^{(n)}, v_{t_j}^{(n)}) + (\gamma v_{t_j}^{(n)} + x_{t_j}^{(n)}) + \gamma \beta^{-1} s_{t_j}^{v(n)}|^2 \Delta t$ 
9:      $t_{j+1} = t_0 + (j+1)\Delta t$  {set time stamp}
10:     $v_{t_{j+1}}^{(n)} = v_{t_j}^{(n)} + \Delta t f_1(t_j, x_{t_j}^{(n)}, v_{t_j}^{(n)})$ ,  $x_{t_{j+1}}^{(n)} = x_{t_j}^{(n)} + \Delta t v_{t_{j+1}}^{(n)}$  {update states}
11:     $s_{t_{j+1}}^{x(n)} = s_{t_j}^{x(n)} - \Delta t \left[ \nabla_x f_1(t_j, x_{t_j}^{(n)}, v_{t_j}^{(n)})^\top s_{t_j}^{v(n)} + \nabla_x (\nabla_v \cdot f_1(t_j, x_{t_j}^{(n)}, v_{t_j}^{(n)})) \right]$ 
12:     $s_{t_{j+1}}^{v(n)} = s_{t_j}^{v(n)} - \Delta t \left[ s_{t_j}^{x(n)} + \nabla_v f_1(t_j, x_{t_j}^{(n)}, v_{t_j}^{(n)})^\top s_{t_j}^{v(n)} + \nabla_x (\nabla_v \cdot f_1(t_j, x_{t_j}^{(n)}, v_{t_j}^{(n)})) \right]$ 
13:   end for
14:   Update  $\theta_m$  through Adam method to minimize Loss
15: end for
16: for  $m = 2, 3, \dots, N_T$  do
17:   Initialize  $\theta_m$  as  $\theta_{m-1}$  from previous stage {warm-start}
18:   for step = 1, 2, ...,  $N_{\text{step}}$  do
19:     Sample  $\{(x_0^{(n)}, v_0^{(n)})\}_{n=0}^{N_x}$  i.i.d. from  $\rho_0$ 
20:     Compute  $s_0^{x(n)} = \nabla_x \log \rho_0(x_0^{(n)}, v_0^{(n)})$  and  $s_0^{v(n)} = \nabla_v \log \rho_0(x_0^{(n)}, v_0^{(n)})$ 
21:     for  $m' = 1, \dots, m-1$  do
22:        $t_0 = (m'-1)T'$  {initial time for the stage}
23:       for  $j = 0, \dots, N_t - 1$  do
24:          $t_{j+1} = ((m'-1)N_t + j + 1)\Delta t$  {set time stamp}
25:          $v_{t_{j+1}}^{(n)} = v_{t_j}^{(n)} + \Delta t f_{m'}(t_j, x_{t_j}^{(n)}, v_{t_j}^{(n)})$ ,  $x_{t_{j+1}}^{(n)} = x_{t_j}^{(n)} + \Delta t v_{t_{j+1}}^{(n)}$  {update states}
26:          $s_{t_{j+1}}^{x(n)} = s_{t_j}^{x(n)} - \Delta t \left[ \nabla_x f_{m'}(t_j, x_{t_j}^{(n)}, v_{t_j}^{(n)})^\top s_{t_j}^{v(n)} + \nabla_x (\nabla_v \cdot f_{m'}(t_j, x_{t_j}^{(n)}, v_{t_j}^{(n)})) \right]$ 
27:          $s_{t_{j+1}}^{v(n)} = s_{t_j}^{v(n)} - \Delta t \left[ s_{t_j}^{x(n)} + \nabla_v f_{m'}(t_j, x_{t_j}^{(n)}, v_{t_j}^{(n)})^\top s_{t_j}^{v(n)} + \nabla_x (\nabla_v \cdot f_{m'}(t_j, x_{t_j}^{(n)}, v_{t_j}^{(n)})) \right]$ 
28:       end for
29:     end for
30:     Loss = 0,  $t_0 = (m-1)T'$ 
31:     Follow steps in line 7-14 to train  $f_m$  with initial data  $\{x_{t_0}^{(n)}, v_{t_0}^{(n)}, s_{t_0}^{x(n)}, s_{t_0}^{v(n)}\}_{n=1}^{N_x}$ 
32:   end for
33: end for

```

Algorithm 4 Flow matching solver for ULD with general potential

```

1: Input: Parameter  $\beta, \gamma$ , neural network structure for each stage, number of steps for
   the first stage  $N_{\text{step0}}$  and the following stages  $N_{\text{step}}$ , learning rates,  $N_x, N_t, N_T$ 
2: Output: Approximated composed velocity fields  $\{f_m(\cdot, \cdot)\}_{m=1}^{N_T}$  for the MFC problem
3: Initialization: Parameter  $\theta_1$  for the first neural network  $f_1(\cdot, \cdot)$ ,  $\Delta t = T/(N_T N_t)$ 
4: for step = 1, 2, ...,  $N_{\text{step0}}$  do
5:   Loss = 0,  $t_0 = 0$ , Sample  $\{(x_0^{(n)}, v_0^{(n)})\}_{n=0}^{N_x}$  i.i.d. from  $\rho_0$ 
6:   Compute  $s_0^{x(n)} = \nabla_x \log \rho_0(x_0^{(n)}, v_0^{(n)})$  and  $s_0^{v(n)} = \nabla_v \log \rho_0(x_0^{(n)}, v_0^{(n)})$ 
7:   for  $j = 0, 1, \dots, N_t - 1$  do
8:     Loss = Loss +  $\frac{1}{N_x} \sum_{n=1}^{N_x} |f_1(t_j, x_{t_j}^{(n)}, v_{t_j}^{(n)}) + (\gamma v_{t_j}^{(n)} + \nabla_x U(x_{t_j}^{(n)})) + \gamma \beta^{-1} s_{t_j}^{v(n)}|^2 \Delta t$ 
9:      $t_{j+1} = t_0 + (j+1)\Delta t$  {set time stamp}
10:     $v_{t_{j+1}}^{(n)} = v_{t_j}^{(n)} + \Delta t f_1(t_j, x_{t_j}^{(n)}, v_{t_j}^{(n)})$ ,  $x_{t_{j+1}}^{(n)} = x_{t_j}^{(n)} + \Delta t v_{t_j}^{(n)}$  {update states}
11:     $s_{t_{j+1}}^{x(n)} = s_{t_j}^{x(n)} - \Delta t \left[ \nabla_x f_1(t_j, x_{t_j}^{(n)}, v_{t_j}^{(n)})^\top s_{t_j}^{v(n)} + \nabla_x (\nabla_v \cdot f_1(t_j, x_{t_j}^{(n)}, v_{t_j}^{(n)})) \right]$ 
12:     $s_{t_{j+1}}^{v(n)} = s_{t_j}^{v(n)} - \Delta t \left[ s_{t_j}^{x(n)} + \nabla_v f_1(t_j, x_{t_j}^{(n)}, v_{t_j}^{(n)})^\top s_{t_j}^{v(n)} + \nabla_x (\nabla_v \cdot f_1(t_j, x_{t_j}^{(n)}, v_{t_j}^{(n)})) \right]$ 
13:   end for
14:   Update  $\theta_m$  through Adam method to minimize Loss
15: end for
16: for  $m = 2, 3, \dots, N_T$  do
17:   Initialize  $\theta_m$  as  $\theta_{m-1}$  from previous stage {warm-start}
18:   for step = 1, 2, ...,  $N_{\text{step}}$  do
19:     Sample  $\{(x_0^{(n)}, v_0^{(n)})\}_{n=0}^{N_x}$  i.i.d. from  $\rho_0$ 
20:     Compute  $s_0^{x(n)} = \nabla_x \log \rho_0(x_0^{(n)}, v_0^{(n)})$  and  $s_0^{v(n)} = \nabla_v \log \rho_0(x_0^{(n)}, v_0^{(n)})$ 
21:     for  $m' = 1, \dots, m-1$  do
22:        $t_0 = (m'-1)T'$  {initial time for the stage}
23:       for  $j = 0, \dots, N_t - 1$  do
24:          $t_{j+1} = ((m'-1)N_t + j + 1)\Delta t$  {set time stamp}
25:          $v_{t_{j+1}}^{(n)} = v_{t_j}^{(n)} + \Delta t f_{m'}(t_j, x_{t_j}^{(n)}, v_{t_j}^{(n)})$ ,  $x_{t_{j+1}}^{(n)} = x_{t_j}^{(n)} + \Delta t v_{t_j}^{(n)}$  {update states}
26:          $s_{t_{j+1}}^{x(n)} = s_{t_j}^{x(n)} - \Delta t \left[ \nabla_x f_{m'}(t_j, x_{t_j}^{(n)}, v_{t_j}^{(n)})^\top s_{t_j}^{v(n)} + \nabla_x (\nabla_v \cdot f_{m'}(t_j, x_{t_j}^{(n)}, v_{t_j}^{(n)})) \right]$ 
27:          $s_{t_{j+1}}^{v(n)} = s_{t_j}^{v(n)} - \Delta t \left[ s_{t_j}^{x(n)} + \nabla_v f_{m'}(t_j, x_{t_j}^{(n)}, v_{t_j}^{(n)})^\top s_{t_j}^{v(n)} + \nabla_x (\nabla_v \cdot f_{m'}(t_j, x_{t_j}^{(n)}, v_{t_j}^{(n)})) \right]$ 
28:       end for
29:     end for
30:     Loss = 0,  $t_0 = (m-1)T'$ 
31:     Follow steps in line 7-14 to train  $f_m$  with initial data  $\{x_{t_0}^{(n)}, v_{t_0}^{(n)}, s_{t_0}^{x(n)}, s_{t_0}^{v(n)}\}_{n=1}^{N_x}$ 
32:   end for
33: end for

```
